Charge-Transfer and Energy-Transfer Processes in π-Conjugated Oligomers and Polymers: A Molecular Picture

Jean-Luc Brédas,*[,†,‡] David Beljonne,[†,‡] Veaceslav Coropceanu,[†] and Jérôme Cornil[†,‡]

School of Chemistry and Biochemistry, Georgia Institute of Technology, Atlanta, Georgia 30332-0400, and Laboratory for Chemistry of Novel Materials, University of Mons-Hainaut, Place du Parc 20, B-7000 Mons, Belgium

Received June 9, 2004

Contents

1. Introduction

Inorganic semiconductor devices such as transistors have been instrumental in shaping the development of our society of information and communication. Recently, the electronics and photonics technologies have opened their materials base to organics, in particular π-conjugated oligomers and polymers. The goal with organics-based devices is not necessarily to attain or exceed the level of performance of inorganic semiconductor technologies (silicon is still the best at the many things that it does) but to benefit from a unique set of characteristics combining the electrical properties of (semi)conductors with the properties typical of plastics, that is, low cost, versatility of chemical synthesis, ease of processing, and flexibility. Interest in conjugated polymers picked up significantly after the 1976 discovery that they can be made highly electrically conducting following a redox chemical treatment.[1] This discovery led to the 2000 Nobel Prize in Chemistry awarded to Alan Heeger, Alan MacDiarmid, and Hideki Shirakawa. By the mid-eighties, many research teams in both academia and industry were investigating π-conjugated oligomers and polymers for their nonlinear optical properties or their semiconducting properties, paving the way to the emergence of the fields of plastic electronics and photonics.[2]

The technological developments in plastic electronics and photonics have been required to gain a much better fundamental understanding of the nature of electronic excitations, charge carriers, and transport phenomena in ordered and disordered π-conjugated materials. Our aim in this contribution is to review a number of these issues and to highlight the fascinating chemistry and physics of these materials and the strong connection that exists in this field between basic and applied research.

A major breakthrough in the field of organic electronics is the 1987 report by Tang and VanSlyke at Kodak of the first electroluminescent device based on a π-conjugated molecular material, tris(8-hydroxyquinoline) aluminum (Alq_3).[3] Shortly thereafter, Friend and his group at Cambridge discovered electroluminescence (EL) in a conjugated polymer, poly(*para*-phenylenevinylene) (PPV), thereby opening the way for the fabrication of polymer light-emitting diodes (LEDs).[4]

Typically, an organic LED is built[5] by successively depositing the following materials on a transparent substrate: a transparent electrode made of a high work function compound, usually indium−tin oxide; one or several organic layers that in the case of molecular materials are generally deposited by vacuum sublimation[6] or in the case of polymers are generally deposited by spin coating or ink-jet print-

* To whom correspondence should be addressed. Tel: 1-404-385-4986. Fax: 1-404-894-7452. E-mail: jean-luc.bredas@chemistry.gatech.edu.
† Georgia Institute of Technology.
‡ University of Mons-Hainaut.

10.1021/cr040084k CCC: $48.50
Published on Web 09/28/2004

Jean-Luc Brédas received his Ph.D. in Chemistry from the University of Namur, Belgium, in 1979. After a joint postdoctoral stay at MIT and the (then) Allied Chemical Corporate Research Center in Morristown, New Jersey, he went back to Namur in 1981 as a Research Fellow of the Belgian National Science Foundation. In 1988, he was appointed Professor at the University of Mons-Hainaut, Belgium, and Head of the Laboratory for Chemistry of Novel Materials. While keeping an Extraordinary Professorship appointment in Mons, Jean-Luc Brédas joined the University of Arizona in 1999 before moving in 2003 to the Georgia Institute of Technology where he is Professor of Chemistry and Biochemistry. He was the recipient of the 1997 Francqui Prize, the 2000 Quinquennial Prize of the Belgian National Science Foundation, the 2001 Italgas Prize for Research and Technological Innovation (shared with Richard Friend), and a member of the team laureate of the 2003 Descartes Prize of the European Union. He is ranked #74 on the list of the 100 most cited chemists for the period January 1993–June 2003. Since 2001, he has been a member of the European Research Advisory Board (EURAB) for Science, Technology, and Innovation. The research interests of his groups focus on the computational design of novel organic materials with remarkable electrical and optical properties.

David Beljonne received his Ph.D. in Chemistry from the University of Mons-Hainaut in 1994. After a postdoctoral stay at the University of Cambridge (with Prof. Sir Richard Friend) and the University of Rochester (with Prof. Shaul Mukamel), he is presently a Senior Research Associate of the Belgian National Science Foundation in Mons and a Visiting Principal Research Scientist at Georgia Tech. His work deals with a theoretical characterization of the nature and dynamics of electronic excitations in conjugated polymers and molecules.

Veaceslav Coropceanu received his Ph.D. in Theoretical and Mathematical Physics from the State University of Moldova in 1985. In 1994, he was appointed as Associate Professor at the same University, with which he was associated until 2004. After research stays at the University of Sussex, United Kingdom (1997–1998) on a NATO/Royal Society Fellowship and at the Medical University of Lübeck, Germany (1999–2000) on an Alexander von Humboldt Fellowship, he joined the Brédas research group in 2000. He is currently a Research Scientist at the Georgia Institute of Technology. His present research interests include the investigation of the electronic properties of organic and inorganic systems, electron-transfer phenomena, and the theory of vibronic coupling.

Jérôme Cornil was born in Charleroi, Belgium, in 1970. He received his Ph.D. in Chemistry from the University of Mons-Hainaut in 1996 and then went for a postdoctoral stay at UCSB (with Alan Heeger) and MIT (with Bob Silbey). He is a Research Associate of the Belgian National Fund for Scientific Research (FNRS) in Mons. He held a Visiting Scientist position at the University in Arizona from 2001 to 2003 and is now a Visiting Principal Research Scientist at the Georgia Institute of Technology. His main research interests deal with the theoretical characterization of the electronic and optical properties of organic conjugated materials used in optoelectronic devices. He is a coauthor of more than 130 publications.

ing;[7] and a top metallic electrode made of a low work function metal or alloy. Four main steps are required to generate light from a LED device upon application of a forward bias, as sketched on the top of Figure 1. (i) Charge injection: Electrons (holes) are injected from the Fermi level of the low (high) work function metal into the lowest unoccupied (highest occupied) electronic levels of the organic material present at the metal−organic interface. (ii) Charge transport: Electrons and holes drift in opposite directions within the organic layer(s) (usually in a dispersive manner) under the influence of the static electric field generated by the forward bias. (iii) Charge recombination: Electrons and holes approaching one another can capture and recombine to lead to the formation of either singlet or triplet excitons; during their lifetimes, excitons can hop among molecules/chains via energy-transfer processes. (iv) Excitation decay: When excitons decay radiatively, the generated light can escape from the device through the transparent side.

In electrophosphorescent diodes, a phosphorescent dye is present as a guest in a host matrix and exciton transfer can take place from the host matrix to the guest; high efficiencies are reached since both singlet and triplet excitations generated in the host can

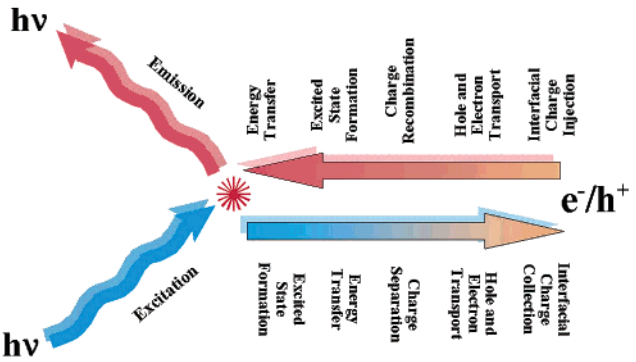

Figure 1. Illustration of the various processes governing the operation of (top) organic LEDS and (bottom) solar cells (adapted from an original sketch by N. R. Armstrong).

transfer to the guest and contribute to the luminescence signal.[8] In conjugated polymer LEDs, in the absence of phosphorescent dyes, only singlet excitons generate light.

Organic LEDs have recently entered the market place as active elements in low-resolution displays such as those commercialized, for instance, by Pioneer in car stereo systems, by Kodak in digital cameras, or by Philips in electric shavers.[9] The production of high-resolution full-color flexible displays for television screens is the next target.

Organic materials are also emerging as promising candidates for the fabrication of transistors, photodiodes and solar cells, and (bio)chemical sensors.[10−13] Photovoltaic devices have an overall architecture similar to that of LEDs; the active organic layers are generally made of two components and sandwiched between two electrodes of a different or the same nature. However, the mode of operation is opposite to that of LEDs, as illustrated on the bottom of Figure 1. The main steps are as follows. (i) Light absorption: Light is absorbed in the organic layers and generates singlet excitons; for solar cells, absorption should match the solar spectrum as closely as possible. (ii) Energy-transfer and exciton dissociation: Excitons have to migrate toward the interfacial region between the organic components; there, they can dissociate, that is, charge separate, as a result of an electron-transfer (ET) process between the donor component and the acceptor component;[12] the efficiency of the charge separation process very much depends on the supramolecular organization at the heterojunction. (iii) Charge transport: The charges that remain separated (and hence do not recombine after exciton dissociation) drift in the organic layers under the influence of the electric field generated by the equalization of the Fermi energy levels of the two electrodes. (iv) Charge collection: The charges have to ultimately be collected at the electrodes.

In organic field effect transistors, the key steps are as follows: (i) formation of a conducting channel within the organic semiconductor due to the application of a gate voltage; upon application of a drain voltage, (ii) charge injection from the source electrode into the organic semiconductor, or (ii) charge transport across the organic layer; and (iii) charge collection at the drain electrode. Charge injection and collection processes actually correspond to redox reactions, that is, ET reactions. Biochemical or chemical sensors based on π-conjugated polymers usually rely on optical absorption, followed by fast energy transfer and charge separation at the quenching (sensing) site.[13]

This brief description of organic (opto-)electronic devices highlights the importance of ET and energy-transfer processes into or within the π-conjugated materials. Thus, the design of new materials with optimal performance requires a fundamental understanding of these processes.

It is useful to point out that both ET and energy-transfer processes are driven by similar electron−electron and electron−vibration interactions. As a result, they can be described by similar mathematical formalisms, a fact especially clear in the case of weak electronic interactions. Both processes can be viewed as special cases of the nonradiative decay of an electronic state. In the framework of perturbation theory,[14,15] the probability for a transition from a discrete initial state ψ_i (corresponding to the reactants) to a discrete final state ψ_f (corresponding to the products of the reaction) writes under application of a perturbation V to first order:

$$P_{if} = \frac{1}{\hbar^2} |\langle \psi_i | V | \psi_f \rangle|^2 \left[\frac{\sin(\omega_{fi} t/2)}{\omega_{fi}/2}\right]^2 \qquad (1)$$

where t denotes time, $\hbar\omega_{fi}$ is the transition energy between the electronic states i and f, and $\langle \psi_i | V | \psi_f \rangle$ is the corresponding electronic coupling matrix element. To account for a continuous distribution of final (vibrationally coupled) electronic states, eq 1 can be recast by introducing the density of final states, $\rho(E_f)$, and summing over all probability densities. Assuming that the function $|\langle \psi_i | V | \psi_f \rangle|^2 \rho(E_f)$ varies slowly with energy, the transition probability per unit time (or transition rate) adopts, in the long-time limit, the simple and widely exploited Fermi's Golden Rule form:

$$k_{if} = \frac{2\pi}{\hbar} |\langle \psi_i | V | \psi_f \rangle|^2 \rho(E_f) \qquad (2)$$

In both electron- and energy-transfer cases, the transition mechanism involves vibrational motions driving the reaction coordinates from reactants to products. The expression for the rate obtained within the Franck−Condon approximation factorizes into an electronic and a vibrational contribution as:

$$k_{if} = \frac{2\pi}{\hbar} |V_{if}|^2 \,(\mathrm{FCWD}) \qquad (3)$$

Here, $V_{if} = \langle \psi_i | V | \psi_f \rangle$ is the electronic coupling matrix element and FCWD denotes the Franck−Condon-weighted density of states. In the high-temperature regime, i.e., when assuming that all vibrational modes are classical ($\hbar\omega_i \ll k_B T$), the FCWD obeys a standard Arrhenius type equation:

$$\mathrm{FCWD} = \sqrt{\frac{1}{4\pi k_B T \lambda}} \exp[-(\Delta G^0 + \lambda)^2/4\lambda k_B T] \qquad (4)$$

and the rate takes its semiclassical Marcus theory expression:[16]

$$k_{if} = \frac{2\pi}{\hbar} |V_{if}|^2 \sqrt{\frac{1}{4\pi k_B T \lambda}} \exp[-(\Delta G^0 + \lambda)^2/4\lambda k_B T] \quad (5)$$

where λ denotes the reorganization energy induced by the electron or the energy transfer and ΔG^0 is the variation of the Gibbs free energy during the reaction. When the reorganization energy λ is cast into contributions of both classical modes for the surrounding medium [(λ_0); $\hbar\omega_h \ll k_B T$] and intramolecular high-frequency vibrational modes [(λ_i); $\hbar\omega_i \gg k_B T$], the rate k_{if} becomes in the context of the Bixon and Jortner model (for details, see the review in ref 15):

$$k_{if} = \frac{2\pi}{\hbar} |V_{if}|^2 \sqrt{\frac{1}{4\pi\lambda_0 k_B T}} \sum_{n=0}^{\infty} \exp(-S_i) \frac{S_i^n}{n!} \exp\left[-\frac{(\Delta G^0 + \lambda_0 + n\hbar\omega_i)^2}{4\lambda_0 k_B T}\right] \quad (6)$$

Here, a single effective quantum mode ω_i is assumed to contribute to λ_i. The Huang−Rhys factor, $S_i = \lambda_i/\hbar\omega_i$, is a measure of the electron−vibrational coupling interaction. The main effect of high-frequency modes is to renormalize the electronic coupling parameter rather than to contribute to the temperature dependence (except at high temperatures). This discussion underlines that to achieve a complete understanding of the electron- or energy-transfer properties, a detailed knowledge of the vibrational modes coupled to the transfer process and of the electron−vibration constants is required.

In this contribution, our main goal is to review some recent work that addresses at the molecular level the nature of the main parameters that govern electron- and energy-transfer processes in π-conjugated oligomers and polymers. This molecular approach contrasts with many models developed earlier for organic materials where these processes have been described on a phenomenological basis and from a macroscopic perspective, thereby masking the actual chemical structures of the systems behind effective parameters.

The structure of this review is as follows: Section 2 deals with reorganization energy and the assessment of electron−vibration constants. In section 3, we address the electronic couplings and charge transport in model systems and in a series of π-conjugated oligomer materials that form single crystalline structures. The following section is devoted to charge recombination in electroluminescent oligomers and polymers, with an emphasis on the rates of formation of the lowest singlet and triplet excited states in *para*-phenylenevinylene chains. Section 5 covers energy transfer in conjugated polymers and discusses the rates for intra- vs interchain migration. Finally, in section 6, we describe some preliminary work on the photoinduced charge-separation process in a two-component organic material system.

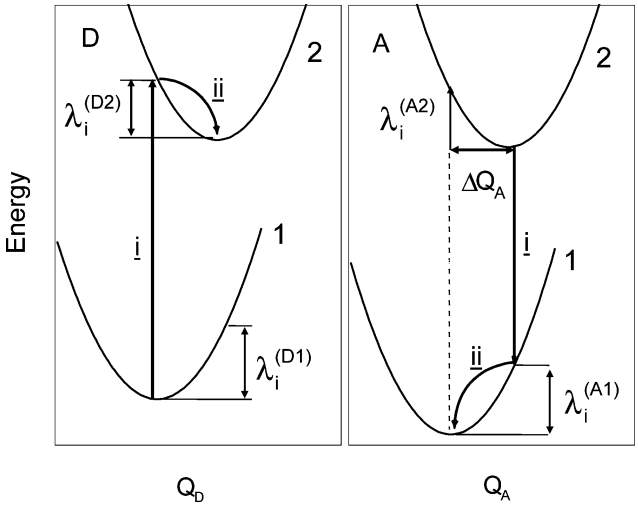

Figure 2. Sketch of the PESs (in the monomer coordinate representation) related to ET, showing the vertical transitions, the NM displacement (ΔQ), and the relaxation energies ($\lambda_i^{(1)}$ and $\lambda_i^{(2)}$).

2. Electron–Vibration Coupling and Reorganization Energy

As emphasized in the Introduction, the reorganization energy is one of the key quantities that control the rates for electron or energy transfer. From the rate expression given in eq 6, it is clear that in the normal regime (i.e., when $|\Delta G°| < \lambda$) the lower the reorganization energy, the higher the rate. Here, we have chosen to discuss mainly the reorganization energy related to electron (charge) transfer, keeping in mind that it has the same physical meaning in both types of processes.

The reorganization energy is usually expressed as the sum of inner and outer contributions. The inner (intramolecular) reorganization energy arises from the change in equilibrium geometry of the donor (D) and acceptor (A) sites consecutive to the gain or loss of electronic charge upon ET. The outer reorganization energy is due to the electronic and nuclear polarization/relaxation of the surrounding medium. It is important to note that due to the weakness of the van der Waals interactions among organic molecules, the separation of the reorganization energy into inter- and intramolecular contributions remains largely valid even in the case of molecular crystals. We note that in most instances the outer contribution to the reorganization energy is expected to be of the same order of magnitude as the inner part (see section 6); it is also expected to be less sensitive to the chemical structure of the constituents than the inner contribution. The formalisms used to estimate the outer reorganization energy have been mainly developed to describe ET processes in solution and apply to isotropic media; thus, it is desirable to extend these standard models to account for the anisotropy in the solid state. In this section, we focus on the intramolecular reorganization energy and its description in terms of vibrational modes.

To illustrate the physical meaning of the intramolecular reorganization energy, we have represented in Figure 2 the potential energy surfaces (PES) of the donor and acceptor involved in an intermolecular ET reaction of the type $D + A^+ \rightarrow D^+ + A$; in the figure,

the electronic states D1 [A1] and D2 [A2] correspond to the neutral and cationic states of the donor [acceptor], respectively. The ET process can be formally divided into two steps: Step i is the simultaneous oxidation of D and reduction of A^+ at frozen reactant geometries (in Figure 2, this step corresponds to a vertical transition from the minimum of the D1 surface to D2 and a similar A2 to A1 transition), and step ii corresponds to the relaxation of the product nuclear geometries.

As seen from Figure 2, the overall intramolecular reorganization energy upon ET consists of two terms:[14−21]

$$\lambda_i = \lambda_i^{(A1)} + \lambda_i^{(D2)} \quad (7)$$

$$\lambda_i^{(A1)} = E^{(A1)}(A^+) - E^{(A1)}(A) \quad (8)$$

$$\lambda_i^{(D2)} = E^{(D2)}(D) - E^{(D2)}(D^+) \quad (9)$$

Here, $E^{(A1)}(A^+)$ and $E^{(A1)}(A)$ are the energies of the neutral acceptor A at the cation geometry and optimal ground-state geometry, respectively, and $E^{(D2)}(D)$ and $E^{(D2)}(D^+)$ are, accordingly, the energies of the radical cation D^+ at the neutral geometry and optimal cation geometry. Equations 7−9 remain valid in the case of an energy-transfer process; the difference is only in the nature of the PESs and the meaning of the D1, D2, A1, and A2 states (λ_i then corresponds, for instance, to the Stokes shift parameter[21]).

The vertical transitions involved in Figure 2 and eqs 7−9 are consequences of the Franck−Condon principle, which requires that the nuclear configurations of the system immediately before and after ET coincide. However, it is important to note that in addition to the Franck−Condon principle, the principle of energy conservation should be also satisfied for ET to occur.[14−16] In the case of optically driven ET, the mismatch between the electronic vertical transitions (see the lines labeled i in Figure 2) is balanced by the absorption of light. In the case of thermal (dark) ET, to satisfy both principles, thermal fluctuations from the equilibrium nuclear configurations of the reactants are needed prior to ET.[16]

2.1. Determination of Reorganization Energy from a Frequency Analysis

The contribution of each vibrational mode to λ_i can be obtained by expanding the potential energies of the neutral and cationic states in a power series of the normal coordinates (denoted here as Q_1 and Q_2). In the harmonic approximation, the relaxation energy λ_i writes[14−21]

$$\lambda_i = \sum \lambda_j = \sum \hbar\,\omega_j S_j \quad (10)$$

$$\lambda_j = \frac{k_j}{2}\Delta Q_j^2,\ S_j = \lambda_j/\hbar\,\omega_j \quad (11)$$

Here, the summations run over the vibrational modes; ΔQ_j represents the displacement along normal mode (NM) j between the equilibrium positions of the two electronic states of interest; k_j and ω_j are the corresponding force constants and vibrational frequencies; S_j denotes the Huang−Rhys factor.

The numerical procedure to obtain the reorganization energy consists of the following steps. First, the NM coordinates and force constants of the electron donor and acceptor are determined. The standard rectilinear NMs $Q_{1(2)}$ are obtained as a linear combination of Cartesian displacements:[22]

$$Q_{1(2)j} = \sum_k L_{1(2)kj}\,[q_{1(2)k} - q_{1(2)k}^{(0)}] \quad (12)$$

The matrix $L_{1(2)}$ connects the $3n$-6 [n is the number of atoms in the (nonlinear) molecule] normal coordinates with the set of $3n$ mass-weighted Cartesian coordinates $q_{1(2)}$; the vectors $q_1^{(0)}$ and $q_2^{(0)}$ correspond to the stationary points on the adiabatic potential surfaces of states 1 and 2, respectively. Then, the NM displacements $\Delta Q_{1(2)}$ are obtained by projecting the displacements $\Delta q = q_1^{(0)} - q_2^{(0)}$ onto the NM vectors. Finally, substituting the calculated quantities into eqs 11, 10, and 7 provides the total relaxation energy.

An alternative and widely applied approach to evaluate the electron−vibration constants is based on the computation of the first derivatives[23−25] of the energy of the states of interest (for instance, the ionized or excited states) with respect to the normal coordinates of a reference configuration. In many applications (see ref 25 for details), this procedure is further simplified by applying the concept of orbital vibronic coupling constants. When attachment or detachment processes are considered (ground state of the charged species), the latter approach is in fact identical to the application of Koopmans' theorem;[26] that is, the derivatives of the energy $E^{(D2)}$ of the radical cation (or radical anion) are approximated by the derivatives of the energy of frontier molecular orbitals (MOs) with respect to the normal coordinates, Q_{1j}, of the ground state (reference configuration). In practice, these quantities are obtained by numerical derivations, performed by distorting the geometry of the neutral molecule along each NM coordinate. We note that when both donor and acceptor possess an orbitally nondegenerate ground state, only totally symmetric vibrations contribute to the relaxation (reorganization) energy.

2.2. Franck−Condon Factor (FCF)

The NMs Q_1 and Q_2 of the neutral and cationic states of the donor (acceptor) are in general related by a transformation consisting of a multidimensional rotation and a translation:[27]

$$Q_1 = JQ_2 + \Delta Q \quad (13)$$

J is the Duschinsky matrix describing the mixing of the normal coordinates of the two states. Therefore, for the calculations of the Franck−Condon integrals (FCIs) entering into eq 3, it is necessary to determine an exact treatment for all four sets of normal coordinates [$Q_{(A1)j}$, $Q_{(A2)j}$, $Q_{(D1)j}$, and $Q_{(D2)j}$]. A significant simplification can be achieved when the donor and acceptor are chemically identical, i.e., in the case of a self-exchange reaction, and when the same force

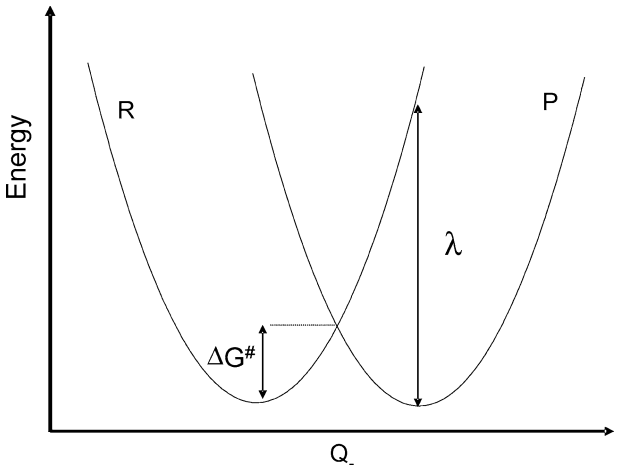

Figure 3. PESs related to ET, in the dimer coordinate representation ($\Delta G° = 0$). The energy barrier $\Delta G^{\#}$ required to reach the transition state and the reorganization energy λ are also illustrated.

constants can be assumed for the cationic and neutral PESs (thus neglecting Duschinski mixing). In such conditions, the energies of the reactants (E_R) and products (E_P) can be written

$$E_R = \sum_j \frac{k_j}{2} [Q_{Dj}^2 + (Q_{Aj} - \Delta Q_j)^2] \quad (14)$$

$$E_P = \sum_j \frac{k_j}{2} [(Q_{Dj} - \Delta Q_j)^2 + Q_{Aj}^2] \quad (15)$$

Applying then a transformation to dimer coordinates,

$$Q_{\pm j} = \frac{1}{\sqrt{2}} (Q_{Dj} \pm Q_{Aj}) \quad (16)$$

it is possible to show that the symmetric dimer coordinates do not couple to the ET reaction. As a consequence, the diabatic (reactant and product) PES can be described by a single set of normal coordinates:[28]

$$E_{P(R)} = \sum_j \frac{k_j}{2} (Q_{-j} \pm Q_0)^2, Q_0 = \Delta Q/\sqrt{2} \quad (17)$$

In the dimer coordinate representation, illustrated in Figure 3, the path for thermal ET can be viewed as a thermal activation of the system from the minimum of curve R to the crossing point of the diabatic curves (R and P) prior to ET, then followed by a relaxation to the equilibrium geometry configuration of the products (minimum of curve P). At the crossing point, the transition is simultaneously vertical and horizontal, thus meeting the requirements of both Franck−Condon and energy-conservation principles.

Both monomer and collective (dimer) coordinate representations are used in practice to describe the transfer processes.[21] In the monomer coordinate representation, the $\langle \psi_i |V| \psi_f \rangle$ matrix element writes

$$\langle \Psi_i^{D1} \Psi_m^{A2} |V| \Psi_j^{D2} \Psi_n^{A1} \rangle = V_{DA} \langle \Phi_i^D | \Phi_J^D \rangle \langle \Phi_m^A | \Phi_n^A \rangle \quad (18)$$

Here, V_{DA} (= V_{if}) is the electronic coupling matrix element and the $\langle \Phi_m(Q) | \Phi_n(Q) \rangle$ terms are the monomer FCIs, given by the overlap of the vibrational functions $\Phi_m(Q_1)$ and $\Phi_n(Q_2)$ of the neutral and cationic ground electronic states, respectively. On the basis of Golden Rule considerations (that is, eq 18), when performing a thermal averaging over the vibrational manifold of the reactants and summing up with respect to all vibrational states of the products, the expression for the rate constant becomes (for mathematical details, see refs 21 and 29):

$$k = \frac{2\pi}{\hbar} V_{DA}^2 \int f_D(E) f_A(E) \, dE \quad (19)$$

The integral in eq 19 represents the FCF; the f_D (f_A) term is related to the emission (absorption) spectrum or the ionization (attachment) spectrum in the case of energy transfer or ET, respectively.[21] This expression for the rate constant is widely applied to describe singlet energy-transfer processes;[21,29] see section 5.

Several methods have been proposed to calculate the multidimensional FCIs, $\langle \Phi_m(Q) | \Phi_n(Q) \rangle$.[30−34] The calculations are considerably simplified when Duschinsky mixing is neglected, i.e., $J = 1$ in eq 13. In this case, referred to as the parallel mode approximation,[30] the FCF of a multidimensional vibrational transition, involving p vibrational modes, is obtained as a simple product of one-dimensional FCIs:[35]

$$FCF(m_1, n_1, m_2, n_2, ..., m_p, n_p) = \prod_{i=1}^{p} FCI(m_i, n_i)^2 \quad (20)$$

$$FCI(m, n)^2 = \exp\{-S\} S^{(n-m)} \frac{m!}{n!} [L_m^{(n-m)}(S)]^2 \quad (21)$$

where $L_n^{\alpha}(x)$ is a Laguerre polynomial. If only transitions from the vibrational ground state ($m = 0$) are considered, the standard Poisson distribution is obtained

$$FCF(m = 0, n) = \frac{S^n}{n!} e^{-S} \quad (22)$$

In the dimer normal coordinate representation, the matrix element $\langle \psi_i |V| \psi_f \rangle$ is defined by only one set of FCIs (also given by eq 20); m and n correspond in such cases to the vibrational levels of the reactant and product states specified by eq 17. Note that in the classical limit the FCF given by eq 20 and averaged by a Boltzmann factor turns into the Marcus expression, eq 5. Considering both high frequency and classical contributions to the reorganization energy leads to eq 6.

2.3. Intramolecular Reorganization Energy of Oligoacene Derivatives

We now describe how we applied the numerical approaches discussed above to the case of oligoacenes

Table 1. Theoretical Estimates of the Relaxation Energies λ_i (meV) and Total Reorganization Energies λ_i^{tot} (meV) of the Oligoacenes, as Obtained from PESs and NM Calculations

	naphthalene	anthracene	tetracene	pentacene
$\lambda_i^{(1)}$ (PES)	94	68	56	48
$\lambda_i^{(2)}$ (PES)	93	69	57	49
λ_i^{tot} (PES)	187	137	113	97
$\lambda_i^{(1)}$ (NM)	98	66	57	51
$\lambda_i^{(2)}$ (NM)	91	70	56	49
λ_i^{tot} (NM)	189	136	113	100

Table 2. DFT/B3LYP Estimates of Frequencies, ω (cm^{-1}), Huang−Rhys Factors, S, and Relaxation Energies, λ_i (meV), for the Totally Symmetric Vibrations of Anthracene in its Neutral and Cation States

neutral			cation		
ω (cm^{-1})	S	λ_i (meV)	ω (cm^{-1})	S	λ_i (meV)
399	0.001	0	396	0.001	0
641	0.000	0	626	0.000	0
766	0.003	0	766	0.002	0
1038	0.002	0	1057	0.000	0
1194	0.021	3	1207	0.026	4
1301	0.048	8	1291	0.019	3
1443	0.094	17	1426	0.150	27
1530	0.010	2	1545	0.048	9
1607	0.194	39	1611	0.127	25
3171	0.000	0	3195	0.000	0
3180	0.000	0	3206	0.000	0
3205	0.001	0	3228	0.000	0
total		69	total		68

containing from two to five rings: naphthalene, anthracene, tetracene, and pentacene.[36,37] These oligomers are of high current interest because of their high charge mobilities in the crystalline state, in particular tetracene, pentacene, and derivatives.[38,39] We note that all calculations including geometry optimizations and NM analyses were performed at the density funtional theory (DFT) level with the hybrid B3LYP functionals using the standard 6-31G** basis set.

The bond-length modifications upon positive ionization show a consistent trend along the series. Naphthalene displays the largest geometry relaxations, with changes in C−C bond lengths on the order of 0.03 Å. This value is reduced to ca. 0.02, 0.015, and 0.01 Å in anthracene, tetracene, and pentacene, respectively. The geometry distortions, as well as the changes in atomic charge densities (Mulliken populations), are found to spread over the entire molecules. The theoretical estimates of the relaxation energies and total reorganization energies obtained from the NM analysis are in excellent agreement with the values computed directly from the adiabatic PESs; see Table 1. The derived values are also in good agreement with the results of previous calculations by Kato and Yamabe and by Klimkans and Larsson.[25,40] Our results indicate that the main contribution to the relaxation energy comes from high-energy vibrations. This high-energy contribution is in fact divided over several vibrational modes with wavenumbers in the range of 1200−1600 cm^{-1}; see Table 2. The contribution to λ_i from low-energy vibrations is negligible in anthracene and tetracene and is very small in the cases of naphthalene and pentacene.

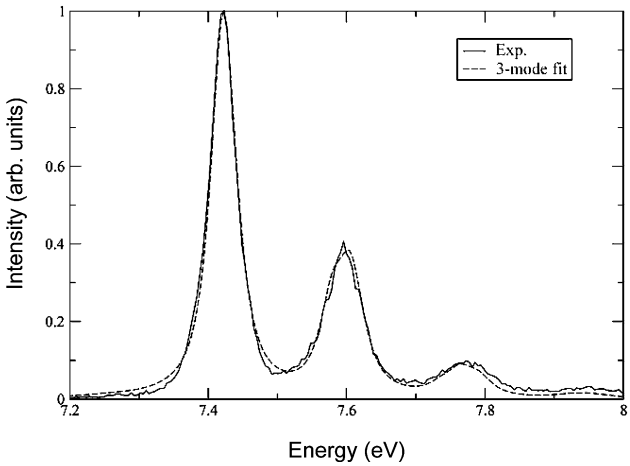

Figure 4. Three-mode fit of the vibrational structure of the first UPS ionization peak of anthracene.

Gas phase UPS was used to estimate the reorganization energy of anthracene, tetracene, and pentacene.[36] The experimental results confirm that the reorganization process in all three systems is dominated by the interaction with rather high-frequency modes, in agreement with the theoretical results. We first fitted the experimental spectrum using vibrational progressions that strictly satisfy the linear vibronic model (eqs 20 and 21). In the fitting procedure, the values of vibrational frequencies and Huang−Rhys factors associated with a vibrational mode are optimized in order to minimize the sum of the squares of the deviations between experimental and computed spectra (using a conventional Levenberg−Marquardt algorithm). Lorentzian functions are used to convolute the transition intensities. We have performed several fits where we increased the number of vibrational modes involved and found that at least three modes were necessary to reproduce accurately the spectral shapes; adding more than three modes did not significantly improve the fit. The fitted spectrum obtained in the case of anthracene is reported in Figure 4. The reorganization energy of 0.174 eV obtained from the fit is somewhat larger than those reported in Table 1 (0.137 and 0.136 eV). The main contribution (97%) to this reorganization energy comes from high-energy vibrations, which lie in the region expected for C−C stretching modes.[37] Similar results are obtained for tetracene and pentacene.

We have also carried out the Franck−Condon simulation of the shape of the first ionization peak of anthracene, tetracene, and pentacene using the DFT/B3LYP estimates of the frequencies and Huang−Rhys factors obtained from NM calculations. The simulations were performed for the temperatures of 372, 452, and 507 K at which the UPS data were collected for anthracene, tetracene, and pentacene, respectively. The position of the 0−0 transitions was chosen to match the maximum of the experimental first ionization peak, corresponding to 7.421 (anthracene), 6.939 (tetracene), and 6.589 (pentacene) eV. A scaling factor, $f = 0.9613$, has been applied to the computed vibrational frequencies, following the recommendations given for the comparison of B3LYP and experimental IR frequencies.[41] The results of the

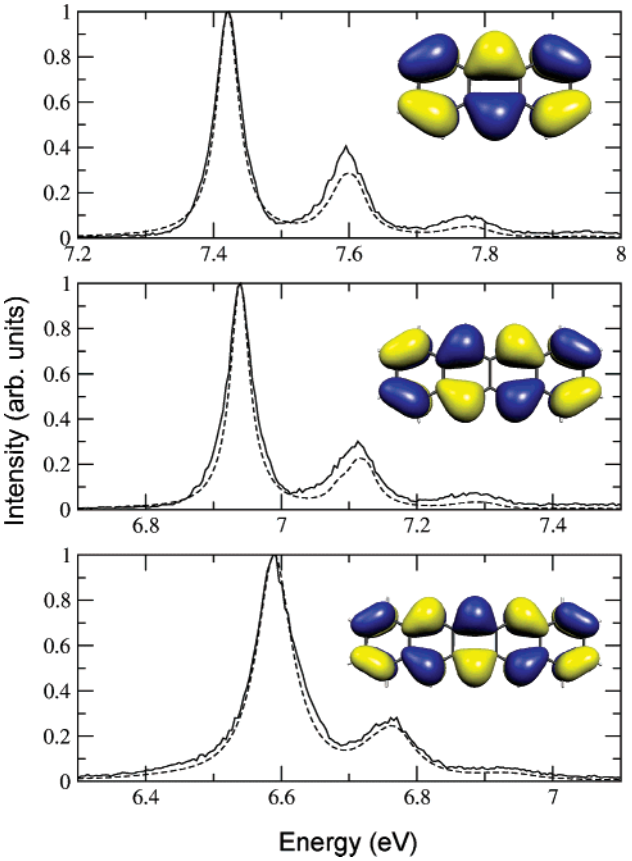

Figure 5. DFT/B3LYP simulation (dashed lines) of the vibrational structure of the UPS first ionization peak of anthracene, tetracene, and pentacene (solid lines). The NMs (eight, seven, and 10 modes for anthracene, tetracene, and pentacene, respectively) of the cation species with the largest Huang−Rhys factors have been used for the simulations. A scaling factor of 0.9613 has been applied to the computed frequencies. The transition intensities were convoluted with Lorentzian functions with full-width at half-maximum (fwhm) of 0.046, 0.046, and 0.060 eV for anthracene, tetracene, and pentacene, respectively. The HOMO wave functions obtained at the DFT/B3LYP level are also illustrated for each molecule.

simulations are shown in Figure 5. In general, the positions and shapes of the peaks are very well-reproduced. For anthracene and tetracene, the intensity of the second peak is slightly underestimated. Nevertheless, taking into account that the parameters have not been adjusted, the overall agreement between simulated and experimental spectra is excellent. Some remaining discrepancy could be due to nonadiabatic interactions, Duschinsky mixing, and anharmonic effects. The calculations of Duschinsky matrices (performed with the DUSHIN program developed by Reimers[17]) point to the presence of some mixing among the vibrations in the 1200−1600 cm^{-1} region; see Table 3. These results suggest that a simulation based on multidimensional FCFs, computed taking into account the Duschinsky mixing, might further improve the agreement between theoretical and experimental spectra. These results underline the importance of multimode effects to obtain a detailed understanding of the UPS band shapes in oligoacenes.

Overall, the intramolecular reorganization energies in tetracene (0.11 eV) and pentacene (0.10 eV) rank among the smallest λ_i values that have been calculated or measured for molecules. The tetracene and pentacene values are about three times as small as in TPD (0.29 eV), which is a hole-transport material widely used in organic molecular devices. Interestingly, side-chain derivatizations of pentacene in the form of ethynylsilyl substitutions have been reported by Anthony and co-workers.[42] We have found that such substitutions actually lead to a significant increase in the intramolecular reorganization energy, by about 50%, due to the involvement of the side chains in the geometry relaxation process upon ionization. In contrast, Wudl and co-workers have recently synthesized a tetra-methyl derivative of pentacene with the goal of improving the processability of the material;[43] these authors calculated the reorganization energy in the same way as described above and obtained that it remains exactly the same as in pentacene; the reason is that, in this instance, the substituents have a saturated nature and do not couple to the geometry relaxations of the conjugated backbone.

The origin of the small reorganization energy values in tetracene and pentacene can be traced back to a combination of macrocyclic rigidity and full delocalization of the frontier MOs;[37] the highest occupied molecular orbital (HOMO) wave functions of anthracene, tetracene, and pentacene are depicted in Figure 5. Accordingly, other molecules that have been found to present small intramolecular λ_i values are fullerenes, as described by Devos and Lannoo,[24] phthalocyanines (Pc),[44] or discotic macrocycles.[45]

We note that the reorganization energy λ_i is directly related to such quantities as the polaron binding energy ($E_{pol} = \lambda_i/2$) and the dimensionless electron−phonon parameter λ_{e-ph} [$\lambda_{e-ph} = \lambda_i N(E_F)$, where $N(E_F)$ is the density of states at the Fermi level].[24,36b] The electron−phonon parameter is a key value in the conventional theory of superconductivity. Therefore, the results discussed above are especially

Table 3. Portion of the A_g Block of the Duschinsky Matrix for Pentacene

		cation								
	ω (cm^{-1})	1338	1425	1441	1515	1560	1590	3192	3196	3202
neutral	1345	−0.967	.196	−0.158	.015	.004	.007			
	1425	−0.197	−0.222	.945	.117	−0.069	.017			
	1448	−0.154	−0.920	−0.237	−0.149	−0.142	−0.162			
	1506	−0.022	.061	.137	−0.953	.181	.188			
	1569	.022	.088	−0.036	−0.092	−0.905	.403			
	1590	−0.023	−0.220	−0.073	.216	.351	.880			
	3166							−0.992	−0.107	.060
	3171							.121	−0.940	.318
	3175							−0.023	−0.323	−0.945

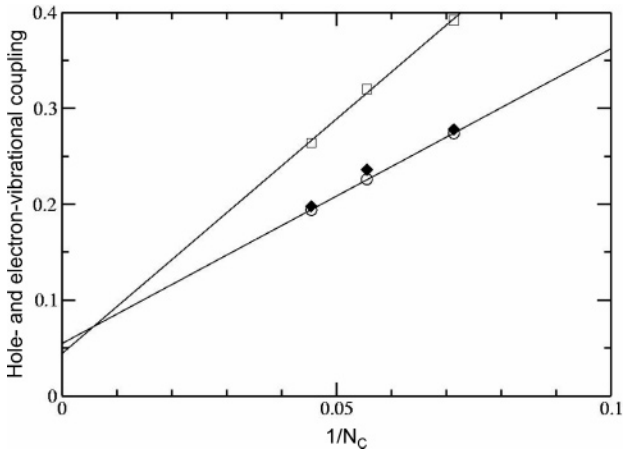

Figure 6. Evolution of the hole−vibrational coupling (open circles) and electron−vibrational coupling (open squares) λ_{e-ph} as a function of the inverse number of carbon atoms in anthracene, tetracene, and pentacene, as calculated at the DFT/B3LYP level. We also report the values deduced for holes from experimental gas phase UPS spectra (black diamonds). The density of states at the Fermi level is set equal to 2 eV^{-1} in all cases.

relevant in the development of adequate polaron models to understand superconductivity and charge transport in organic molecular systems. In Figure 6, we compare the electron−vibration constants calculated for electrons and holes in the anthracene, tetracene, and pentacene series. The constants are found to be larger for electrons than holes; however, the difference decreases with chain length and would vanish in (hypothetical) long acene oligomers (unless charge localization, i.e., polaron formation, starts occurring in long oligomers).

3. Electronic Coupling and Charge Transport

The charge transport properties in conjugated materials critically depend on the packing of the chains and order in the solid state as well as on the density of impurities and structural defects. As a result, the measured mobility values can largely vary as a function of sample quality.[46] Overall, the transport mechanism results from a balance between the energy gained by electron delocalization in an electronic band and the energy gained by geometry relaxation of an individual chain around a charge to form a polaron; the latter term is often referred to as the relaxation (binding) energy of the polaron.[47]

In highly purified molecular single crystals such as pentacene, transport at low temperature can be described within a band picture, as shown by Karl and co-workers.[48] As a general rule of thumb, (effective) bandwidths of at least 0.1 eV are needed to stabilize a band regime.[47] In that case, the positive or negative charge carriers are fully delocalized and their mobilities are a function of the width of the valence or conduction band, respectively, i.e., of the extent of electronic coupling between oligomer chains. In pentacene, low-temperature charge carrier mobilities of up to 60 cm^2/Vs have been reported.[49] When the temperature increases, the mobilities progressively decrease as a result of scattering processes due mainly to lattice phonons, as is the case in metallic conductors; transport can then be described on the basis of effective bandwidths that are smaller than the bandwidths obtained for a rigid lattice. At an elevated temperature, transport operates via a thermally assisted polaron hopping regime where localized charge carriers jump between adjacent chains, as described, for instance, by Conwell and co-workers.[50]

The hopping regime generally applies in the presence of significant static disorder, dynamic fluctuations, and/or impurities. For instance, it is expected to operate in spin-coated or ink-jet-printed thin films used in polymer devices or in liquid crystalline materials.[51] At the microscopic level, polaron hopping can be viewed as a self-exchange ET reaction where a charge hops from an ionized oligomer to an adjacent neutral oligomer, as described in the Introduction; see eqs 5 and 6 with $\Delta G^0 = 0$. In that context, the carrier mobilities are a direct function of the ET rates that, as was described above, are determined by two major parameters: (i) the electronic coupling V_{if} between adjacent chains, which needs to be maximized; in the present context, the electronic coupling is often assimilated to the transfer integral, t, between adjacent chains; and (ii) the reorganization energy λ, which needs to be minimized.

As we described several aspects related to reorganization energy in the previous section, here, we turn most of our attention to the characteristics of the electronic coupling between adjacent π-conjugated chains.

A number of computational techniques, based on ab initio or semiempirical methodologies, have been developed to estimate the electronic coupling V_{if}; they have recently been reviewed in refs 14, 15, and 52. A robust approach to compute V_{if} is to describe the diabatic states of the reactants and products by means of a Slater determinant and to compute their splitting at the transition state;[53] this approach has been applied by He and co-workers to benzene and biphenyl dimers using concerted linear reaction coordinates to define the geometry of the transition state.[53] Another approach is to use Koopmans' theorem and to estimate (in the context of a one-electron picture) the transfer integrals (t) for holes (electrons) as half the splitting of the HOMO (lowest unoccupied molecular orbital, LUMO) levels in a system made of two chains in the neutral state. In the case of benzene and biphenyl dimers, a good quantitative agreement is observed between the two approaches, except in the strongly interacting regime (that we will not be considering here), expected to take place in the case of small molecules separated by short intermolecular distances.[53] The applicability of Koopmans' theorem was confirmed in a study by Pati and Karna.[54] It is also worth mentioning that the transfer integrals can be estimated in a yet simpler approach from the spatial overlap between the two atomic orbitals in interaction.[55,56] All of these considerations explain that many theoretical studies have made use of Koopmans' theorem to estimate electronic couplings.[55−61]

We note that much care has to be taken when Koopmans' theorem is used to estimate the transfer

integrals in asymmetric dimers. In such instances, part of the electronic splitting can simply arise from the different local environments experienced by the two interacting molecules, which create an offset between their HOMO and LUMO levels. To evaluate the effective couplings, this offset can be accounted for by performing calculations using MOs localized on the individual units as basis set[62] or by applying an electric field to promote the resonance between the electronic levels, as done by Jortner and coworkers;[59] however, in the case of weakly polar molecules, these site energy fluctuations are typically small as compared to the transfer integrals and will not be considered hereafter.

The electronic splittings reported below have been calculated within Koopmans' theorem using the semiempirical Hartree−Fock INDO (intermediate neglect of differential overlap) method; interestingly, the INDO method typically provides transfer integrals of the same order of magnitude as those obtained with DFT-based approaches.[45,63] It is of interest to note that when building (infinite) one-dimensional stacks of chains, the widths of the corresponding valence and conduction bands are usually found to be (nearly) equal to four times their respective t integrals; this indicates that in most instances the tight-binding approximation is relevant. Below, we first discuss transfer integrals in model systems before dealing with crystalline structures.

3.1. Model Systems

A first insight into what impacts intermolecular/interchain transfer integrals can be obtained by taking the simple case of a system made of two polyene chains exactly superimposed on top of one another, that is, in a cofacial configuration.[51] Figure 7a illustrates the evolution of the electronic splitting associated to the HOMO and LUMO levels as a function of the number of double bonds along the conjugated backbone. It is observed that (i) the HOMO splitting is systematically larger than the LUMO splitting and (ii) the HOMO splitting decreases with chain length while the LUMO splitting displays the opposite behavior.

These observations can be rationalized by first looking at the nature of the frontier electronic levels for two ethylene molecules in a cofacial configuration; see Figure 7b. In the isolated ethylene molecule, the HOMO level displays a fully bonding pattern where the lobes of the same sign of the two π-atomic orbitals overlap, while the LUMO level corresponds to the antibonding situation where lobes of opposite sign overlap (thereby introducing a node in the electronic wave function in the middle of the bond). When the two molecules interact, the HOMO and LUMO each split into two levels. The magnitude of the HOMO splitting is very large, 0.54 eV for an intermolecular distance of 4 Å; the reason is that the interaction between the two molecules gives rise to interchain overlaps that are fully constructive/bonding for the lower level and destructive/antibonding for the upper level; see Figure 7b. The splitting is much smaller for the LUMO level (0.15 eV) since the antibonding

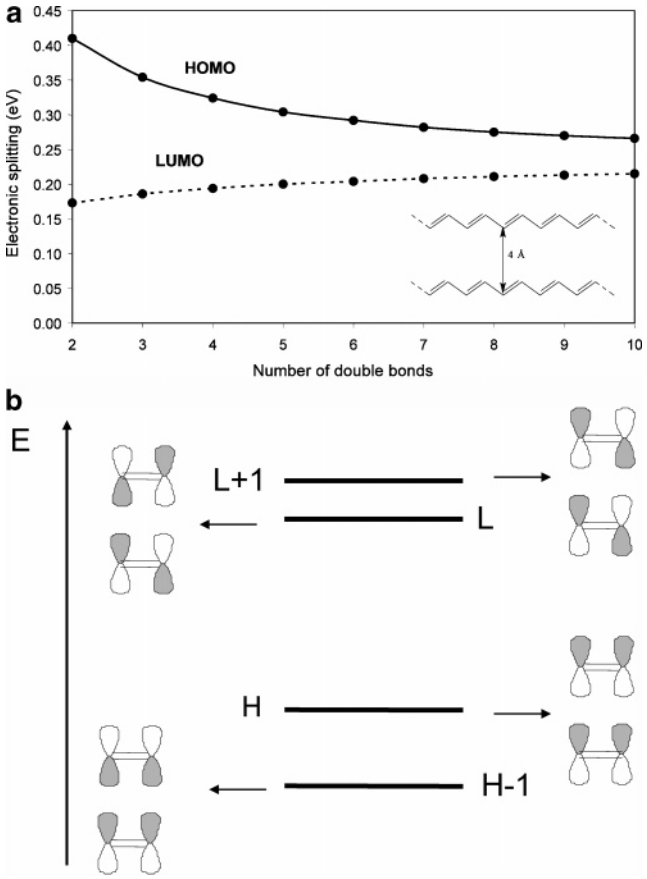

Figure 7. (a) INDO evolution of the HOMO and LUMO splittings in cofacial systems made of two polyene chains separated by 4 Å as a function of the number of double bonds along the conjugated path. (b) Illustration of the bonding vs antibonding intermolecular interactions between the HOMO [LUMO] levels of two ethylene molecules in a cofacial configuration.

character associated to the LUMO level of the isolated molecule yields a mixing of bonding and antibonding interchain overlaps: there occur "direct" bonding interactions (by direct interactions, we mean those between π-atomic orbitals that are exactly superimposed) that are compensated by "diagonal" antibonding interactions in the lower level; in the upper level, "direct" antibonding interactions are compensated by "diagonal" bonding interactions. Thus, the presence of a node in the LUMO wave function is responsible for the smaller electronic splitting. Observation (i) is then understood on the basis that in polyene chains the LUMO wave function always has one extra node with respect to the HOMO wave function. This conclusion actually holds true for conjugated systems with a similar distribution of electronic density in the HOMO and LUMO levels (electron−hole symmetry); this is the case, for instance, in oligothiophenes, oligophenylenes, oligoarylene vinylenes, and their derivatives.

Observation (ii) can be explained by realizing that in going from ethylene to butadiene, the HOMO (LUMO) level of the isolated butadiene molecule acquires some antibonding (bonding) character; in a

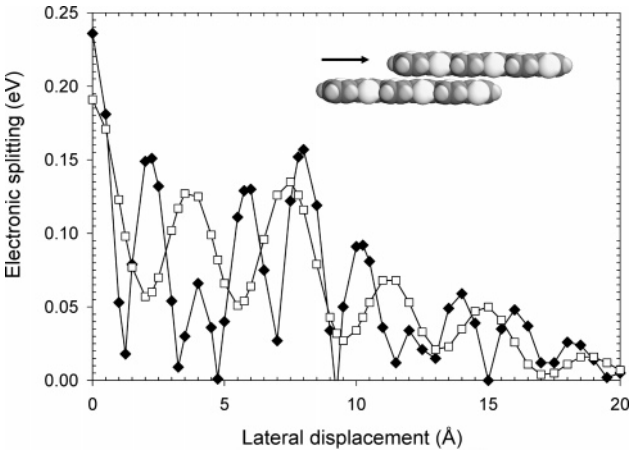

Figure 8. INDO evolution of the absolute value of the electronic splitting for the HOMO (filled diamonds) and LUMO (open squares) in a system formed by two 6T chains in a parallel displaced configuration, as a function of the degree of translation of the upper chain. Note that the lotal length of a 6T molecule is about 22 Å.

cofacially interacting system, this leads to the appearance of "diagonal" antibonding (bonding) interactions that contribute to decrease (increase) the HOMO (LUMO) splitting. The HOMO and LUMO splittings converge toward the same value for long chains since the impact of a single node difference between the HOMO and the LUMO levels attenuates with increasing chain length.

Three important characteristics can be underlined from this simple analysis of perfectly cofacial configurations.[51] (i) By their very nature, cofacial configurations provide the largest electronic interactions (coupling) between adjacent chains. (ii) As a qualitative rule, the lower the number of nodes in the wave function of the frontier level of an isolated chain, the larger the splitting of that level upon cofacial interaction. (iii) In cofacial stacks of oligomers, the valence bandwidth is expected to be larger for small oligomers and the conduction bandwidth is expected to be larger for long oligomers; however, for any oligomer length, the valence bandwidth remains larger than the conduction bandwidth. The latter point is the basic reason that it has generally been considered that organic materials should display higher hole mobilities than electron mobilities.

However, perfectly cofacial configurations are hardly encountered in actual crystalline structures. As soon as we move away from such ideal structures, the situation becomes much more complex.[51] As an example, we have examined the influence of the relative positions of two interacting oligomers by translating one of them along its long molecular axis. Figure 8 displays the evolution of the absolute values for the HOMO and LUMO electronic splittings in two interacting sexithienyl (6T) chains where the top oligomer is translated along its main chain axis while keeping the molecular planes parallel to one another.

Figure 8 illustrates the appearance of strong oscillations in the $2t$ (splitting) values, with a periodicity that is about twice as small for the HOMO splitting as for the LUMO splitting; it also confirms that the largest electronic splittings are calculated for the fully cofacial configurations. The important consequence of the difference in oscillation periods for the HOMO and the LUMO is that small translations can lead to situations where the electronic splitting becomes larger for the LUMO than for the HOMO. For instance, for a displacement of about 1.5 Å along the long chain axis, the reversal in the relative amplitude of the splittings is very significant: we calculate a LUMO splitting about six times as large as the HOMO splitting (0.12 vs 0.02 eV). In such instances, because the conduction bandwidths in oligomer stacks are larger than the valence bandwidths, electrons can be expected to be intrinsically more mobile than holes (provided the reorganization energies in both cases are similar). Thus, this result contrasts with the conventional wisdom expressed earlier that in crystals or crystalline thin films of π-conjugated chains, hole mobility should always be larger than electron mobility.

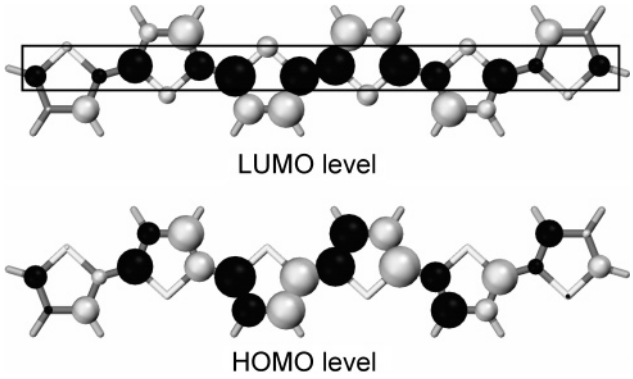

Figure 9. Illustration of the LCAO bonding−antibonding pattern of the HOMO (bottom) and LUMO (top) levels in the 6T molecule. The color and size of the circles are representative of the sign and amplitude of the LCAO coefficients, respectively.

The calculated evolutions can once again be rationalized from the shape of the HOMO and LUMO orbitals found in the isolated 6T molecule. In the HOMO level, the distribution of the positive and negative LCAO (linear combination of atomic orbitals) coefficients shows a change in the sign of the wave function every half monomer unit; see Figure 9. This pattern thus leads to maxima in the calculated electronic splittings for degrees of translation corresponding to multiples of half the monomer unit size. In contrast, the minima are calculated for geometries where the double bonds of one oligomer are superimposed over the center of the thiophene rings or the inter-ring bonds of the other chain; in such configurations, the global overlap (and hence the HOMO splitting) is considerably reduced by the compensation of bonding and antibonding interactions between the double bonds of one chain and the two adjacent double bonds of the other chain. In the LUMO level, there is no change in the sign of the LCAO coefficients along the translation axis. This pattern systematically leads to dominant bonding (antibonding) overlaps in the LUMO (LUMO + 1) level of the interacting system and, hence, to significant electronic splittings; this explains why the minima do not reach values as low as in the HOMO evolution. Maxima (minima) are observed when the thiophene rings of one chain overlap the thiophene

rings (the inter-ring bonds) of the second chain; the oscillation period of the curve is thus twice as large as that calculated for the HOMO splitting. Note that the overall decrease in the HOMO and LUMO splittings for increasing translational shifts simply results from the progressive reduction in the overall extent of spatial overlap between the two oligomers.

The configuration where one oligomer is rotated by 180° along the long-chain axis is also of interest. In this case, the molecular planes are still fully parallel but superimposed rings point in opposite directions ("anti-cofacial" configuration). Taking an interchain distance of 4 Å, the rotated geometry displays calculated splittings of 0.08 and 0.14 eV for the HOMO and LUMO levels, respectively, to be compared with 0.24 and 0.19 eV for the cofacial geometry. The LUMO splitting has a similar order of magnitude in the two configurations due to the fact that the interactions between the β-carbon atoms in the cofacial configuration are compensated by the interactions between the sulfur atoms and the C−C single bonds in the rotated geometry. In contrast, the absence of electronic density on the sulfur atoms in the HOMO level prevents a similar compensation from occurring and leads to a significant reduction in HOMO splitting when going from cofacial to rotated geometry. Thus, this points to another type of configuration for which stacks could present larger conduction bandwidths than valence bandwidths.

This discussion illustrates that the amplitudes of the transfer integrals depend on both the relative positions of the interacting molecules/oligomers and the shape (bonding−antibonding pattern) of their frontier MOs. Thus, the transfer integral amplitudes can hardly be predicted from a simple examination of molecular packing; this underlines the useful role that quantum chemistry can play by providing a molecular-scale understanding of the charge-transport parameters in conjugated systems. We can further illustrate this point by considering an example related to discotic liquid crystalline molecules. Following the pioneering work of Ringsdorf, Haarer, and co-workers,[64] discotic liquid crystals, such as those based on triphenylenes and derivatives, currently emerge as promising materials for use in organic electronic devices; they can display high carrier mobilities due to their spontaneous organization into one-dimensional columns and their self-healing properties.

Figure 10 describes the HOMO and LUMO splittings for two triphenylene molecules separated by 3.5 Å in a cofacial geometry and their evolutions when rotating one molecule around the stacking axis. The splittings are maximized in the eclipsed (cofacial) conformations and reach vanishingly small values for angles of 60, 180, and 300°, which (as a consequence of the D_{3h} symmetry of the triphenylene molecule) result in the lowest degree of interaction between the wave functions of the two disks.[45,65] Along discotic columns (stacks), there often occur significant deviations from cofacial geometries, namely, in order to minimize the steric interactions among the lateral chains introduced to promote the liquid crystalline character. Thus, such deviations can be highly detrimental for charge mobilities, especially if the molecules are locked in conformations that correspond to the lowest splittings. At first sight, the oscillatory evolution of the transfer integrals calculated for triphenylene and derivatives could be attributed to the presence of voids between the external rings of the conjugated cores. However, this interpretation is inconsistent with the fact that the same kind of oscillations is obtained for hexabenzocoronene (HBC), which presents a filled disc-shaped core; see Figure 10[66]; in this case, minima are calculated at multiples of 60° rotations due to the D_{6h} symmetry of HBC. These results again illustrate that the amplitude of the transfer integrals is governed not only by the shape of the molecules but also by the shape of the wave functions of the frontier electronic levels. We note that quantum-chemical calculations have been used to design, prior to synthesis, new discotic mesogens whose transport properties are affected by such rotations to a much lesser extent. This is the case, for instance, for hexaazatriisothianaphthenes[67] and triphenylene derivatives incorporating nitrogen atoms in the external rings.[45,65]

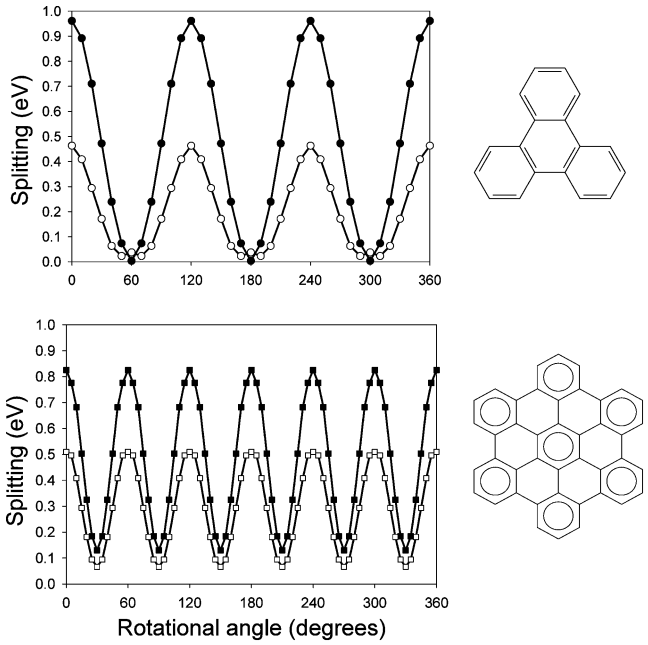

Figure 10. Evolution of the INDO-calculated electronic splittings of the HOMO (filled symbols) and LUMO (open symbols) levels in systems formed by two triphenylene (top) and HBC (bottom) molecules separated by 3.5 Å, as a function of the rotational angle between the two molecules.

3.2. Crystalline Structures

We now turn to a discussion of a series of conjugated materials of interest for their use in organic field-effect transistors, 6T, bisdithienothiophene (BDT), and oligoacenes, and describe their interchain transfer integrals on the basis of their actual crystal packing. The single crystals of 6T in both the low-temperature[68] and the high-temperature[69] phases and of oligoacenes[70−73] are characterized by a layered structure; within these layers, the molecules pack in a herringbone fashion. At first sight, such a molecular arrangement would be expected to lead to only weak overlap between the electronic wave functions of

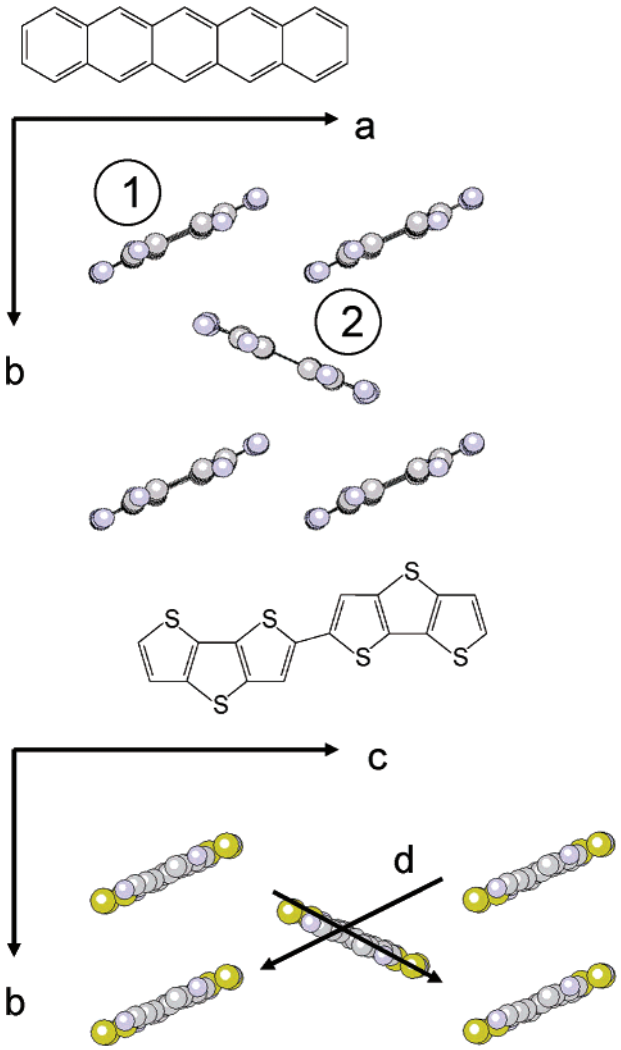

Figure 11. Illustration of the crystal packing of pentacene (top) and BDT (bottom). We display here the layout of the molecules within one layer. Labels 1 and 2 refer to the inequivalent molecules in the unit cell of pentacene.

adjacent chains since their molecular planes tend to being nearly perpendicular to one another. In contrast, the crystal structure of BDT[74] displays a strong orbital overlap for molecules stacked along the *b*-axis (see Figure 11); this is expected to impact the transport properties and bring significant differences with respect to 6T and oligoacenes.

Note that there are two different molecules (labeled 1 and 2 in Figure 11) within the layers of the pentacene single crystals considered here, as reported in ref 72. These two molecules have slightly different geometries; as a result, there exists a difference in the energy of the HOMO and LUMO levels of the inequivalent molecules. This difference has to be accounted for when determining the valence and conduction bandwidths in the crystals.[75] For two interacting chains, the effective transfer integrals (that are lower than the apparent values) can be determined in the framework of a tight-binding formalism as:

$$2t' = \sqrt{4t^2 - (E_1 - E_2)^2} \qquad (23)$$

where t' and t are the effective and apparent inter-

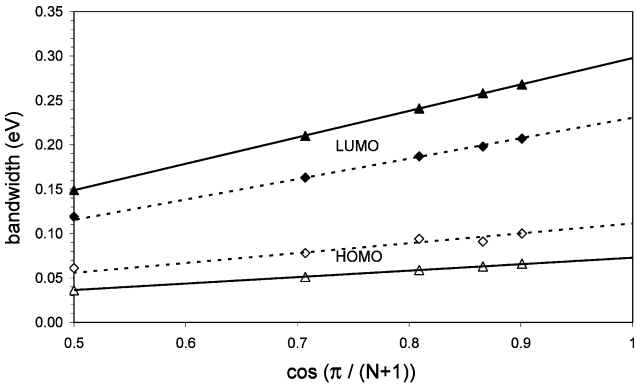

Figure 12. Evolution of the INDO bandwidths formed by the HOMO (open symbols) and LUMO (filled symbols) levels of 6T molecules stacked along the *a*-axis (solid lines) and the diagonal axis *d* (dashed lines), as a function of cos($\pi/N + 1$), with *N* the number of molecules in the clusters.

chain transfer integrals, respectively, and $E_1 - E_2$ denotes the energy offset between the HOMO or the LUMO levels of the two chains.

In the oligoacene and 6T crystal structures, the transfer integrals between molecules in adjacent layers (i.e., for example, along the *c*-axis in pentacene) are negligible. As a result, charge transport is expected to take place predominantly within the layers, which is in agreement with experiment.[76,77] This implies that the achievement of high carrier mobilities in field-effect transistors requires a proper orientation of the layers within the semiconductor channel. In the oligoacene and 6T single crystals, significant electronic splittings arise along the axis connecting cofacially displaced molecules (i.e., the *a*-axis in the pentacene crystal; see Figure 11) and the diagonal axes *d* along the herringbone (illustrated in the case of BDT in Figure 11).

We first discuss the 6T crystal and consider one-dimensional clusters formed by 6T chains stacked along either the *a*- or the *d*-axis and built from the low-temperature crystalline phase. Figure 12 shows the evolution of the bandwidth formed by the interacting HOMO and LUMO levels, as a function of cos($\pi/N + 1$), with *N* being the number of chains in the stacks. The results show that (i) despite the herringbone arrangement, the splittings are significant along the *d*-axes. (ii) The electronic splittings saturate rapidly with cluster size. (iii) There appears to be a very good linear relationship between the splittings and cos($\pi/N + 1$), as would be expected in the framework of tight-binding models including only nearest-neighbor interactions. Thus, the valence and conduction bandwitdhs of 6T infinite one-dimensional stacks can be simply obtained as twice the HOMO and LUMO splittings calculated for two interacting chains. (iv) The splitting of the LUMO level is systematically larger than that calculated for the HOMO level, in contrast to the situation found for perfectly cofacial configurations. This behavior can be rationalized from the shapes of the HOMO and LUMO wave functions and the relative orientations of the interacting units.[51] Thus, in a band regime or in the presence of similar reorganization energy effects, electrons can be expected to be intrinsically more mobile than holes in the 6T single crystal.

Table 4. Total Bandwidth (in meV) of the Valence and Conduction Bands in the Single Crystal of Oligoacenes Containing from Two to Five Rings, as Estimated from the Three-Dimensional Band Structure Generated at the INDO Level

	naphthalene	anthracene	tetracene	pentacene
valence	409.00	509.40	625.50	738.40
conduction	372.30	508.30	502.70	728.00

However, mobility measurements on 6T thin films and crystals reveal a predominant hole transport; this is attributed to extrinsic effects, related in particular to oxygen/water contamination (with oxygen/water acting as electron traps).[76]

Taking account of the layered structure, a total width of 240 meV is calculated for the valence band in the low-temperature phase, to be compared with a 50−100 meV value deduced from mobility measurements.[78] The total valence bandwidth in the high-temperature phase of the 6T crystal is calculated to be larger (328 meV) than in the low-temperature phase, thereby illustrating the subtle interplay between chain packing and interchain transfer integrals. Band-structure calculations based on the extended Hückel formalism by Haddon and co-workers give a value of 420 meV for 6T in the high-temperature phase[79] while values of 0.17 and 0.45 eV are obtained for 4T in the low and high temperature phases, respectively;[80] similarly, large band dispersions (on the order of 0.5 eV) have been obtained at the DFT level for substituted oligothiophenes[81] as well as for oligophenylenes.[82]

In the case of the oligoacene single crystals, the evaluation of the three-dimensional band structures based on the INDO-calculated splittings between adjacent chains leads to very significant bandwidths for both the valence and the conduction bands; see Table 4.[75] The results indicate the following: (i) The electronic splittings are very similar for electrons and holes, in contrast to the situation in crystalline 6T. (ii) Both the HOMO and the LUMO splittings increase with molecular size, in contrast to the evolution found in cofacial geometries (vide supra). (iii) The bandwidths are very significant and range from 300 meV in naphthalene to 700 meV in pentacene. This compares very well with the bandwidths obtained at the DFT level for pentacene;[83a] in contrast, the bandwidths obtained with the extended Hückel formalism are 2−3 times smaller.[83b]

These results are consistent with the achievement of a band regime at low temperature in perfectly ordered and purified oligoacene crystals. Importantly, in pentacene, there occurs an interesting combination of large bandwidths with small reorganization energies, as described in the previous section. This suggests that the band regime could be operative up to relatively high temperatures; very recent measurements on ultrapurified crystals actually show hole mobilities at room temperature as large as 35 cm^2/Vs.[49]

It is worth noting that the valence and conduction bands of the single crystals considered here are actually made of two subbands of different widths since the unit cell contains two inequivalent molecules. The hole (electron) mobility then depends on the curvature of the top (bottom) of the upper (lower) band in the valence (conduction) band, or to first approximation, on the width of these subbands. While the widths of the total valence and conduction bands are very similar in the pentacene single crystal (around 730 meV), the upper occupied and lower unoccupied subbands are 523 and 183 meV wide, respectively.[75] This suggests that in the band regime, hole mobility is larger than electron mobility; the same is expected in the hopping regime, since we pointed out at the end of the previous section that the electron−vibration couplings are larger than the hole−vibration couplings; see Figure 6.

The charge transport properties are markedly different in the BDT single crystal since the molecules are packed along the *b*-axis in nearly cofacial configurations. Significant electronic splittings are calculated only along the *b*-axis and there occur much larger interchain transfer integrals between the HOMO levels than between the LUMO levels (172 vs 27 meV). The theoretical splittings follow a cosine relationship vs *N* and provide by extrapolation valence and conduction bandwidths of 688 and 108 meV, respectively.[51] Charge transport in the BDT single crystal has thus a one-dimensional character with holes expected to be much more mobile than electrons.

To conclude this section, we underline that combining the results of calculations on transfer integrals (electronic couplings) and on intramolecular reorganization energies (electron− and hole−vibration constants) provides very useful trends regarding the intrinsic electron and hole mobilities in π-conjugated materials. However, to be in a position to estimate carrier mobilities at the molecular level, the role of the interactions with lattice phonons and of the induced electronic polarization needs to be incorporated, as shown in a number of recent studies.[84]

4. Charge Recombination in Electroluminescent Oligomers and Polymers

From our discussion in the Introduction, it is clear that the efficiency of organic LEDs depends to a large extent on the nature of the excited species that are formed upon recombination of injected positive and negative charges. These excitations are known to be a function of both electron−vibration and electron−electron interactions; they are generally believed to be excitons with a binding energy in excess of kT.[85]

Of importance is that singlet and triplet excitons possess different energies; the singlet−triplet energy difference, that is the exchange energy, is estimated to be larger than half an electron-volt for the lowest excitation in a range of conjugated polymers.[86−90] They also display different geometry relaxations; because of the possibility of exchange between like spins, triplet wave functions usually display a more spatially confined character, a feature that is especially pronounced for low-lying excitations.[91] As we discuss below, the different nature of the singlet and triplet excitations has a profound impact on the theoretical upper limit for the quantum yields achievable in LEDs.

The quantum efficiency for EL (photoluminescence, PL), η_{EL} (η_{PL}), is defined as the ratio between the number of photons coming out of the device and the number of electrons injected (photons absorbed). In π-conjugated oligomers and polymers, the ratio η_{EL}/η_{PL} is controlled by the fraction of singlet excitons generated in the diode (hereafter referred to as η_2). For a long time, this ratio was thought to follow simple spin multiplicity rules according to which η_{EL}/η_{PL} should not exceed 25% (since the recombination of an electron−hole pair—both spin l/2—leads to a total of four microstates with three triplet states and one singlet state). However, although the issue remains somewhat controversial,[92] there is now compelling experimental[93−98] and theoretical[99−103] evidence that in conjugated polymers, larger ratios between EL and PL quantum yields can be achieved. This stresses the possibility of producing highly efficient polymer LEDs and raises fundamental questions about the mechanisms determining exciton formation, which form the topic of this section.

Cao et al. found that upon improving the electron transport properties of a substituted PPV-based LED device, the ratio of external quantum efficiencies of EL with respect to PL can reach a value as high as 50%.[93] Values of η_2 ranging from 0.35 to 0.45 have also been reported by Ho et al. in PPV derivatives.[94a] Wohlgenannt et al. have measured η_2 by using a photoinduced absorption detected magnetic resonance technique for a large number of π-conjugated polymers and oligomers; the experimental η_2 values were found to increase with conjugation length ranging from ∼0.25 in monomers to much larger values in extended π-conjugated systems.[95] Similarly, Wilson et al. have reported a singlet generation fraction close to 57% in a platinum-containing conjugated polymer, while a much smaller value (22%) was inferred for the corresponding monomer.[94b] The recent work at Philips is especially important in this regard and suggests quantum yields on the order of 60% in polymer LEDs based on polyparaphenylene vinylene or polyspirobifluorenes.[98] From these experimental data, the emerging picture is that η_2 follows closely spin statistics in small conjugated oligomers or molecules[104] while the 25% statistical limit can be significantly overcome in polymers.

Charge recombination between an injected electron and an injected hole appears to occur as a two-step process.[97] In a first step, the initially fully separated charges coalesce into loosely bound singlet or triplet polaron pairs, also referred to as charge-transfer (CT) excitons. In a second step, these intermediate states then decay into lower singlet or triplet neutral exciton states. Two major aspects need to be emphasized. (i) Because the first step can only obey spin statistics, when the second step is faster than any other process affecting the intermediate CT states, spin statistics is followed. Thus, overcoming spin statistics requires that the second step be significantly slower for triplet than for singlet CT states. Then, either of two things can happen. Intersystem crossing can switch triplet pairs into singlet pairs[105,106] that could decay down the singlet exciton manifold, or triplet pairs can have time to dissociate, and some of the freed charges can later reassociate as singlet pairs. (ii) Baessler and co-workers[107] have recently shown, via thermoluminescence measurements on phenylene-based materials, that the singlet−triplet splitting among the CT states (polaron pairs) is merely on the order of 3−6 meV (depending on polymer morphology); thus, the possibility exists for intersystem crossing or possibly dissociation of the CT states.

If we denote by σ_S and σ_T the cross-sections for formation of neutral singlet and triplet exciton states, the expression for η_2 can be written as:

$$\eta_2 = \sigma_S/(\sigma_S + 3\sigma_T) = \sigma_{S/T}(\sigma_{S/T} + 3) \qquad (24)$$

where $\sigma_{S/T} = \sigma_S/\sigma_T$. For $\sigma_S = \sigma_T$, we get $\eta_2 = 25\%$, the statistical limit; η_2 becomes 50% for $\sigma_S = 3\sigma_T$; for $\sigma_T = 0$, $\eta_2 = 100\%$.

Bittner and co-workers have developed a methodology based on the particle−hole picture of solid state physics that allows the simulation of the dissipative dynamics of an extended one-dimensional polymer system coupled to a phonon bath.[100,101] When applying this formalism to a quantum molecular dynamics simulation of the formation of exciton states from polaron pairs, they found a clear correlation between the rates for intrachain generation of singlet and triplet excitons on a single long PPV segment and the corresponding binding energy: the ratio σ_S/σ_T was calculated to evolve linearly with the singlet to triplet binding energy ratio.[101] This evolution was explained in terms of spin specific energetics and mutual vibronic couplings between the excited states on an isolated polymer chain. Below, it is argued that the rate-limiting step is the interchain charge recombination process from the CT states into the manifold of intrachain singlet and triplet excitons (followed by faster downhill internal conversion driven by vibronic couplings). Mazumdar and co-workers also reported chain length-dependent formation cross-sections for interchain charge recombination, based on exact calculations for small polyene chains.[102]

We now discuss the results of calculations aimed at exploring the chain length dependence of the singlet and triplet formation cross-sections in conjugated materials.[108] It is important to stress that both the electronic couplings and the energetics of the charge recombination process were accounted for in this work by applying a standard Jortner formulation for the calculation of charge recombination rates.[15] Different generation rates are obtained for the singlet and triplet excitons due to the different nature of these excited states, which impacts their relative energies and gives rise to different electronic tunneling matrix elements for charge recombination. Most importantly, the formation rates of singlet over triplet neutral excitons are found to vary significantly with chain length.

4.1. Theoretical Aspects

The σ_S and σ_T cross-sections can be calculated in the framework of perturbation theory and the Fermi Golden Rule, as described in the Introduction. To compute the electronic coupling V_{if}, the singlet and triplet excited-state wave functions were obtained for

unrelaxed geometries by combining a Pariser−Parr−Pople (PPP) Hamiltonian to a single configuration interaction (SCI) scheme. The lowest-lying CT state is taken as the initial state in the recombination process; this state is described by a single determinant built by promoting an electron from the HOMO of one chain to the LUMO of an adjacent chain. This is reasonable since the electron (hole) can relax from higher unoccupied (lower occupied) orbitals to the lowest (highest) one, prior to recombination. To account for the polarization effects induced by the medium, the energies of the excitonic and polaronic species were computed at the AM1(CI) level within the continuum dielectric approximation through the use of a COSMO approach.[109] We also considered the Coulomb stabilization E_{cb} of the initial state in the recombination process, which in the model corresponds to a pair of opposite charges lying on adjacent conjugated segments; this stabilization can be estimated on the basis of the charge density distributions in the positive and negative polarons:

$$E_{cb} = \sum_i \sum_j \frac{q_i q_j}{\epsilon_s r_{ij}} \quad (25)$$

where q_i (q_j) is the charge on site i (j) in the positively (negatively) charged molecule, as calculated with a Mulliken population analysis at the AM1/CI-COSMO level, and r_{ij} is the distance between sites i and j; ϵ_s is the medium static dielectric constant, which is taken in both eq 25 and the COSMO calculations to be equal to 4, a typical value for the dielectric constant of organic conjugated polymers.[110,111] The energy separation between the initial charge-separated state and the lowest excited state for the singlet process then writes

$$\Delta_S = E(P^+) + E(P^-) - 2 \times E(S_0) - E(S_1) + E_{cb} \quad (26)$$

where $E(P^+)$, $E(P^-)$, $E(S_0)$, and $E(S_1)$ correspond to the energies in their relaxed geometries of the positive and negative polarons and the singlet ground and excited states, respectively. Note that Δ_S is the driving force, ΔG^0, for the charge recombination reaction into S_1; the changes in Gibbs free energy relative to the processes yielding higher-lying singlet S_n states or triplet T_n excited states are obtained by adding to Δ_S the $S_n - S_1$ or $T_n - S_1$ energy difference as provided by the PPP/SCI scheme (for such processes, the entropy effects can be neglected).

We considered a two-chain model with two possible orientations for the conjugated chains; see top of Figures 13 and 14. While "interchain" electron or hole hopping between adjacent chains lying in a cofacial (or, more generally, H-type) arrangement is the most likely scenario in short chains, migration of the charges between conjugated segments on the same chain is also possible in longer (polymer) chains; the head-to-tail configuration in Figure 14 is intended to model such an "intrachain" process. The calculations were performed on phenyl-capped phenylene vinylene oligomers ranging in size from two to 10 phenylene rings; hereafter, we only refer to the results obtained

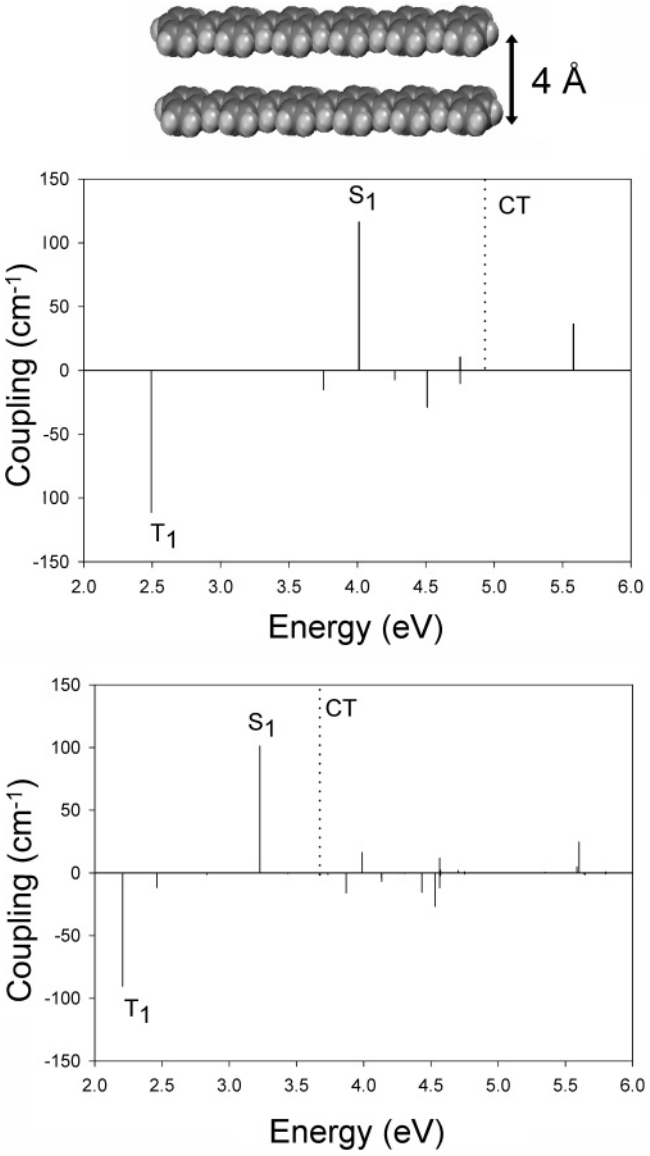

Figure 13. Charge recombination electronic couplings, V_{if}, into singlet and triplet excited states in cofacial dimers of OPV2 (middle) and OPV6 (bottom) molecules. For the sake of clarity, V_{if} values are reported as positive and negative values for singlets and triplets, respectively. The PPP/SCI excitation energies from the singlet ground state to the lowest singlet and triplet excited states are shown on the abscissa axis. The approximate energetic position of the lowest charge-separated state, as obtained from AM1/CI/COSMO calculations, is indicated by the dashed line. The molecular packing is shown on top.

for oligomers containing two rings, OPV2 (the *trans*-stilbene molecule) and six rings, OPV6; these are taken as representatives for "small molecules" and "polymer chains", respectively.

4.2. Chain Length Dependence of Singlet and Triplet Exciton Formation Rates

The spin-dependent recombination process from CT states to neutral exciton states (the second step described above) can be depicted as an ET reaction. Thus, in the context of eq 6, we will discuss consecutively the impact of (i) the electronic couplings (matrix elements), V_{if}; (ii) the driving force, ΔG^0; and (iii) the inner and outer reorganization energies, λ.

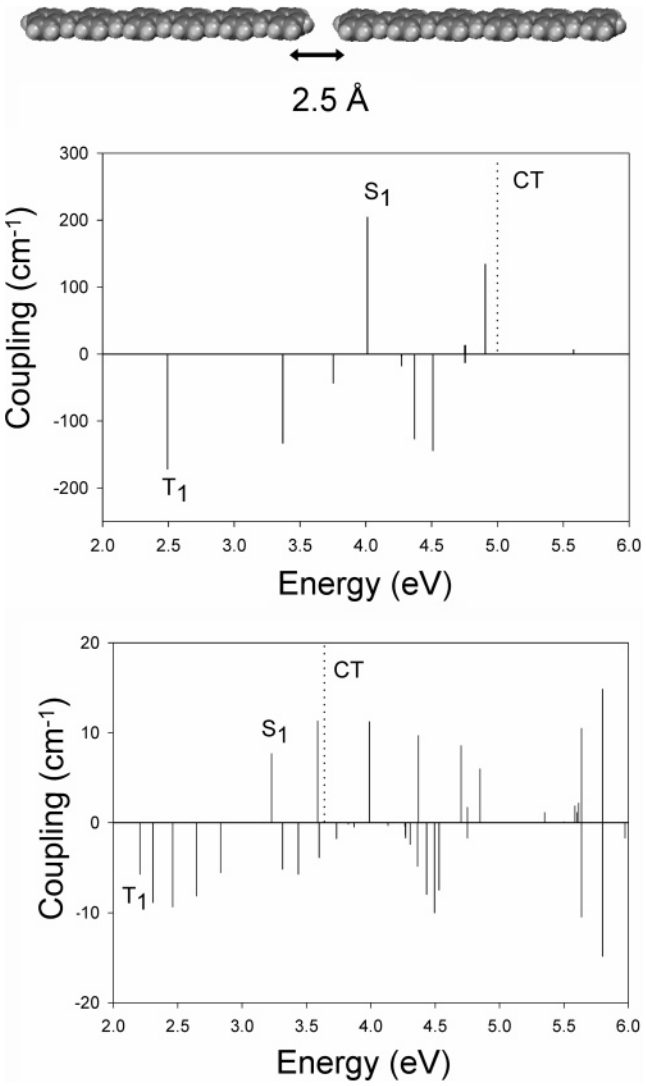

Figure 14. Charge recombination electronic couplings, V_{if}, into singlet and triplet excited states in head-to-tail dimers of OPV2 (middle) and OPV6 (bottom) molecules. Note the change in scale for the couplings (by a factor of 15) between OPV2 and OPV6. The molecular packing is shown on top.

4.2.1. Electronic Couplings

The main results are collected in Figures 13 and 14, which show the electronic couplings between the CT states and the singlet and triplet excitons as a function of excitation energy, and in Figure 15, which displays the evolution with chain length of the ratio between the electronic couplings into S_1 and T_1.

In the cofacial arrangements, the largest matrix elements are calculated for the lowest singlet S_1 and triplet T_1 excited states, in agreement with previous works.[99,102] This feature can be readily explained on the basis of the overlap between the wave functions of the initial and final states. Because the initial CT state is assumed to be a pure transition from the HOMO of one chain to the LUMO of the other chain, optimal overlap is achieved with the final excited state that involves the largest contributions from these frontier orbitals, i.e., the lowest-lying singlet and triplet states. Note that the system in the cofacial arrangement possesses C_{2h} symmetry; only B_u symmetry excited states are then allowed to couple electronically to the B_u symmetry CT state.

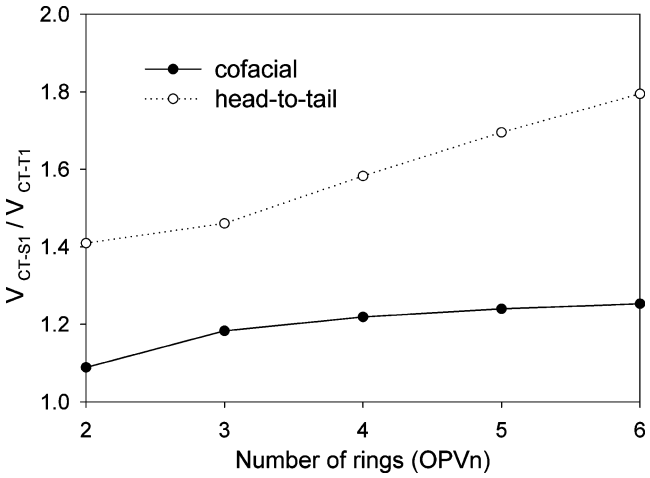

Figure 15. Evolution with chain length of the ratio between the exciton formation electronic couplings, V_{if}, into the lowest singlet and triplet excited states, in cofacial (solid line) and head-to-tail (dashed line) configurations.

The situation is somewhat different for the head-to-tail configurations, where a number of different singlet and triplet excited states show significant electronic couplings to the CT state; this is partly due to the reduced symmetry of the head-to-tail arrangement. Here, chain-end contributions to the wave functions play a major role. A clear correlation can be found between the magnitude of the interchain matrix elements and the shape of the excited-state wave functions, with more delocalized excited states leading to larger couplings.

While in cofacial aggregates the ratio between the matrix elements for charge recombination to yield S_1 vs T_1 is hardly chain length-dependent, the corresponding ratio shows a marked increase in the case of head-to-tail arrangements. This comes from the different nature of the lowest singlet and triplet excited states, the latter being more localized around the central part of the chain.[91] As expected, the differences in the spatial confinements of the S_1 and T_1 wave functions are amplified in the head-to-tail configurations for which contributions at the edges of the conjugated segments are the most relevant.

It is useful to recall that electronic excitations in phenylene-based materials can be classified into three categories, depending on the nature of the involved MOs:[112,113] *dd** excitations, built by promoting an electron from an occupied delocalized MO to an empty delocalized MO; *ll** excitations, involving only orbitals that are localized on the phenylene rings; and *dl**/*ld** excitations, which correspond to transitions from occupied delocalized orbitals to unoccupied localized orbitals and vice versa.

Figure 13 indicates that in cofacial aggregates there is a series of excited states, lying about 4.0−5.0 eV above the ground state, with recombination matrix elements on the order 10−30 cm^{-1}; in this spectral range, singlet and triplet excited states show similar electronic couplings, although slightly larger for the triplets. These high-lying excited states are assigned mainly to mixed *dl**/*ld** and, to a lesser extent, *ll** type excitations. Because of their reduced electron−hole overlap, the singlet and triplet *dl**/*ld** excited states are almost degenerate, display similar

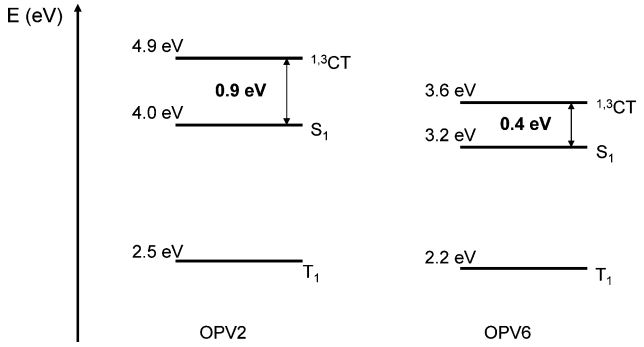

Figure 16. Schematic energy diagram showing the position of the lowest on-chain singlet, S_1, and triplet, T_1, excited states and the lowest charge-separated states, ^{1}CT and ^{3}CT, in a cofacial stack made of two OPV2 and OPV6 oligomers.

wave functions, and hence lead to nearly equal charge recombination cross-sections. As described below, these states could play an important role in the exciton formation mechanism in small molecules. In head-to-tail configurations, Figure 14, the situation is more complex; higher-lying *dd** excitations acquire significant coupling with the CT state as a result of the lower symmetry of the dimers and close contacts between the edges of the conjugated segments. It should be noted that the magnitude of the electronic couplings drops much more quickly with chain length in head-to-tail vs cofacial dimers, a feature that has also been underlined in the case of excitonic energy-transfer processes.[114]

4.2.2. Driving Force

Figure 16 provides a schematic energy diagram with the relevant electronic states for the OPV2 and OPV6 model systems (assuming a distance between the molecular planes of 4 Å in a cofacial dimer). For both chains, the lowest intrachain singlet excited state lies below the charge-separated state, which is consistent with the view that primary photoexcitations in PPV are on-chain excitations and not polaron pairs.[115,116] The most important result is that the energy gap Δ_S between S_1 and ^{1}CT decreases significantly when going from OPV2 ($\Delta_S \sim 0.9$ eV) to OPV6 ($\Delta_S \sim 0.4$ eV).

4.2.3. Reorganization Energy

The inner part, λ_i, corresponds to the energy required to switch from the geometry of two oppositely charged polarons (forming the CT state) to the equilibrium geometry of the target excited state on one chain and the ground-state geometry on the other chain. Because of the close similitude of the geometric distortions induced by charge injection or neutral excitation in a conjugated chain (at least for the lowest singlet excited state),[117] we expect this contribution to be on the order of the polaron relaxation energy. We have therefore chosen a λ_i value of 0.15 eV, which together with an effective frequency mode of 0.15 eV leads to a Huang−Rhys factor $S = 1$. Because of the low dielectric constant of organics and the short separation between the positive and the negative charges in the CT state, the solvent contribution to the relaxation energy ought also to

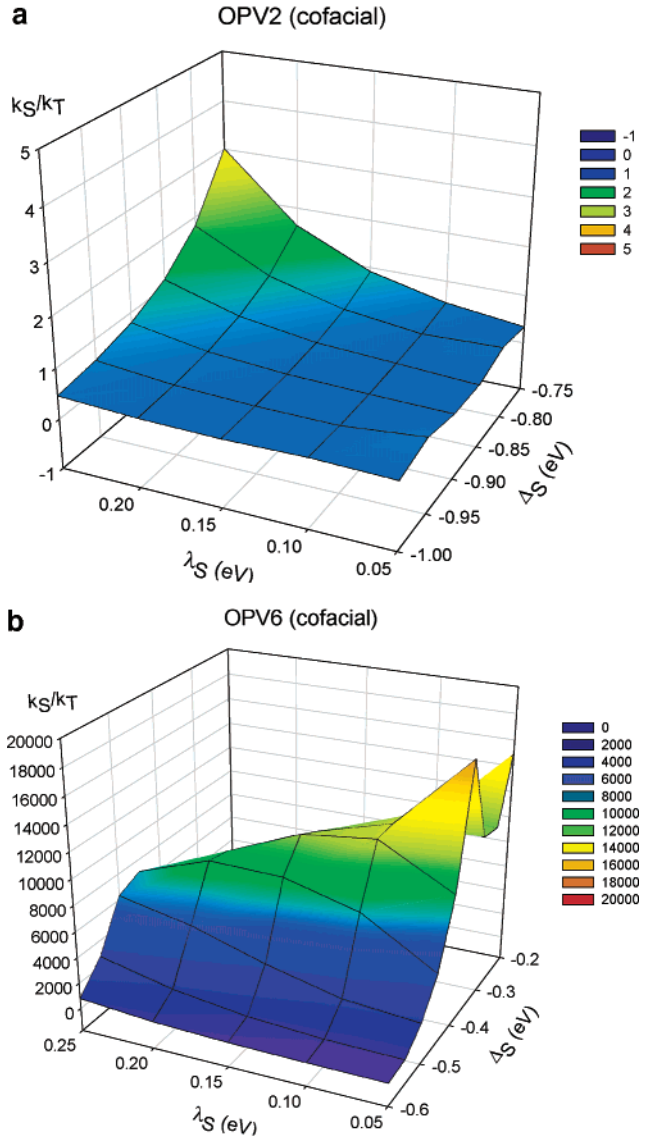

Figure 17. Ratio between the singlet and the triplet charge recombination rates, $r = k_S/k_T$, as a function of Δ_S and λ_S, in a cofacial arrangement of two OPV2 (a) and OPV6 (b) chains.

be small, on the order of that found in weakly polar solvents, typically a few tenths of an electron-volt.

The different approximations that we were forced to take do not allow quantitative predictions of the exciton formation rates. However, we have made sure that the choice of molecular parameters used in the simulations does not affect the overall picture, by applying eq 6 to a range of λ_s and Δ_S values. The resulting ratios between singlet and triplet exciton generation rates, $r = k_S/k_T$ (where k corresponds to the sum over all pathways in a given manifold), are reported as two-dimensional grids in Figures 17 and 18. As expected, the absolute values of the rates are very sensitive to the relative magnitude of the driving force with respect to the reorganization energy, which according to a classical view fixes the height of the barrier for the recombination reaction. However, the important results are the following: (i) For most of the $\{\lambda_s, \Delta_S\}$ space explored, the k_S/k_T ratio is smaller or close to one in OPV2 while it is much higher in OPV6 (especially in the cofacial configuration). (ii)

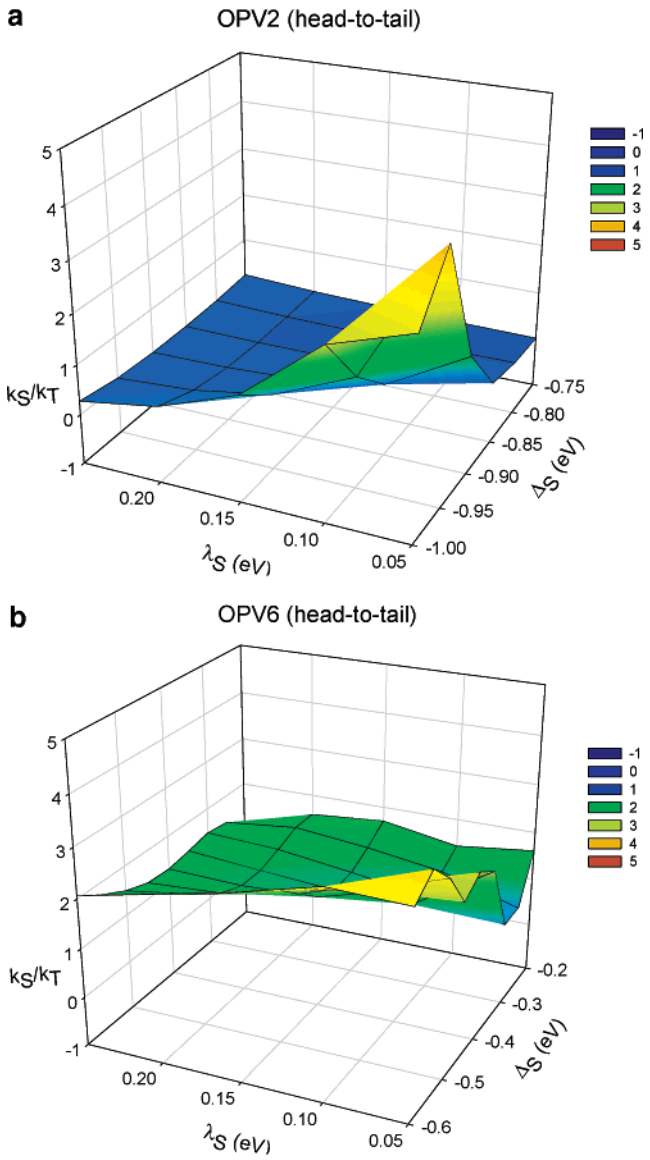

Figure 18. Ratio between the singlet and the triplet charge recombination rates, $r = k_S/k_T$, as a function of Δ_S and λ_S, in a head-to-tail arrangement of two OPV2 (a) and OPV6 (b) chains.

Despite the relatively small electronic couplings, the calculated recombination rates at room temperature are relatively fast (they somewhat vary as a function of the actual values chosen for the reorganization energy and driving force): in OPV2, on the order of 10^9-10^{10} s^{-1} for both singlets and triplets, and in OPV6, ca. $10^{10}-10^{11}$ s^{-1} for singlets but significantly smaller, 10^7-10^8 s^{-1}, for triplets.

These results can be understood in the following way. For small molecules in a face-to-face arrangement, the rather large energy separation between the CT state and the lowest singlet excited state reduces the efficiency of the direct S_1 generation. In this case, higher-lying singlet S_n states, closer in energy and electronically coupled to the initial CT state, are formed with a higher probability; these include the *dl**/*ld** excitations. Because these excited states are only weakly split by exchange interactions, the corresponding triplet T_n excited states have comparable excitation energies, wave functions, electronic couplings, and therefore recombination rates. It follows that in short oligomers, singlets and triplets form with comparable probabilities and spin statistics is pretty much obeyed. In contrast, the S_1 pathway is dominant in long chains due to the reduced $S_1-{}^1CT$ energy gap and the larger tunneling matrix element associated to that state. Because S_1 shows the largest electronic coupling, the singlet route is favored over the triplet channel in extended systems; this results in ratios between singlet and triplet formation rates largely exceeding one. The situation is more complex in head-to-tail arrangements where higher-lying *dd** excited states also play a significant role. In all cases, direct formation of T_1 is very unlikely due to the very large change in Gibbs free energy (on the order of 1.5 eV in OPV6 and larger than 2 eV in OPV2), which sets this process into the inverted Marcus region.[118]

While the mechanism proposed above specifically applies to phenylene-based materials (for which different types of excitations are encountered), the results can be generalized to a number of other conjugated polymers. Indeed, in the simplest one-dimensional two-band model (such as the one used to describe the excited states in polyenes),[119] the average electron−hole separation of the on-chain excitations goes up with increasing energy. Hence, high-lying excited states are less subject to exchange interactions, which decay exponentially with distance. Because it can be reasonably expected that only these higher-energy states are reached efficiently in small molecules or oligomers, this will result in singlet and triplet formation rates of comparable magnitudes. In extended π-systems, contributions from the lowest excited state should dominate the mechanism of singlet generation, because of both large electronic recombination matrix elements and small energy barriers. This process is expected to occur at a faster rate than the formation of any triplet T_n excited state; hence, neutral triplet excitons should be created at a lower rate than singlets, opening the way to deviations from spin statistics.

Using transient spectroscopic techniques, Wohlgenannt et al. have measured the formation cross-section ratio of singlet and triplet excitons in a variety of π-conjugated materials.[96] They found a universal relationship between the low-energy polaron absorption and the chain length in oligomers and, on that basis, showed that the larger the conjugation length, the higher the singlet population. Their experimental data also indicate that the formation cross-section ratio increases in the following sequence: 6T (sexithiophene) < PPE (polyparaphenyleneethynylene) < PPV < RRaP3HT (regio-random polyhexylthiophene) < mLPPP (ladder type polyparaphenylene) < RR-P3HT (regioregular polyhexylthiophene). This trend might be due to material-dependent Δ_S values (i.e., the energy separation between S_1 and the lowest CT or polaron pair state), rather than changes in the singlet exciton binding energy (i.e., the energy difference between S_1 and the single particle continuum). Δ_S is very sensitive not only to the chemical structure of the individual conjugated chains but also to the way the chains pack in the solid state, with the lowest values found in the

most highly ordered materials. The largest ratios between singlet and triplet yields measured for RR-P3HT and mLPPP suggest that small Δ_S values (these two materials display a high degree of both intrachain and interchain order) translate into efficient singlet generation.

In this section, the mechanisms of singlet and triplet exciton formation in electroluminescent π-conjugated materials have been explored. The main conclusions can be drawn as follows: (i) Deviations from simple spin statistics (according to which only one-fourth of excitons are formed as singlets) can occur if triplet CT excited states (polaron pairs) are amenable to intersystem crossing or dissociation. (ii) The electronic couplings between the CT states and the neutral exciton states are predicted to be largest for S_1 and T_1. However, because of the large exchange energy K ($S_1 - T_1$ energy difference), the probability for direct recombination into T_1 is, in all cases, very small (Marcus inverted regime). (iii) In small molecules, the CT$-S_1$ energy difference is large. Both singlet and triplet exciton formations proceed via higher-lying S_n/T_n states, which display similar electronic couplings and are therefore characterized by similar formation rates. These rates are fast, and as a result, spin statistics is expected to be obeyed. (iv) In extended conjugated chains, the energy difference between the CT and the S_1 excited states becomes on the order of the reorganization energy, i.e., a few tenths of an electron-volt; in a Marcus picture, this leads to the smallest barriers. As a result, the ^{1}CT $\rightarrow S_1$ pathway tends to be even faster than in small molecules. On the contrary, the ^{3}CT $\rightarrow T_n$ channels become much slower, leaving room for intersystem crossing or dissociation among the ^{3}CT states.

In a simplified picture, these results suggest that making the energy separation between the CT state and the lowest singlet exciton state smaller can increase the relative generation of singlets vs triplets. It would follow that highly ordered materials (with short intermolecular contacts and delocalized charges) should have the largest singlet/triplet ratios. However, this does not necessarily imply that the highest quantum yields could be reached. Indeed, by reducing the energy separation between intrachain and interchain excitations, the relative population of nonemissive polaron pair species should also increase, which could potentially impact the balance between radiative and nonradiative decay channels. Thus, there is a need to develop materials where an optimal compromise can be achieved between singlet exciton generation and luminescence efficiency.

5. Energy-Transfer Processes in Conjugated Materials

Energy transfer is a key process in the operation of a number of optoelectronic devices based on conjugated materials. In addition, a striking demonstration of ultrafast energy transfer in conjugated polymers is the discovery by Chen et al. of highly sensitive biological and chemical sensors based on reversible fluorescence quenching in a polyanionic PPV.[120] The use of a conjugated polymer was found to lead to a greater than one million-fold amplification of the sensitivity to luminescence quenching, relative to that of small molecules with similar structures. Among others, this work and that of Swager and co-workers[13] have raised a considerable interest in developing a detailed understanding of the mechanisms for energy migration in conjugated polymers. One of the main issues concerns the relative efficiencies of interchain vs intrachain energy-transfer processes. This problem has been elegantly tackled by Schwartz and co-workers; these authors have shown that when alkoxy-substituted PPV is placed in an environment where interchain interactions are inhibited (through incorporation of single conjugated chains in the pores of a silica matrix), exciton diffusion along the chain is slow due to weak dipole coupling of the excitations along the chain direction.[121]

In the present context, intrachain energy migration means hopping of electronic excitations along a single polymer chain with a rigid rodlike conformation, thus in the absence of any chain−chain contact. Depending on the chemical structure of the conjugated polymer and on its "history" (sample preparation parameters, nature of solvent, etc.), various conformations can form such as defect cylinder or defect coil where $\pi-\pi$ interactions can arise from the collapse of single conjugated chains.[122] For instance, experimental investigations using single-molecule spectroscopy have suggested the presence of multiple funnels associated to chain folding in an alkoxy PPV derivative; these funnels form "a landscape for pseudo intrachain energy transfer", which drives the excitons toward quenching sites.[122] When chain−chain contacts do not prevail, deexcitation of single molecules mainly involves migration of the excitons along the conjugated chains and radiative decay of the excited species.

Guest−host systems are also attractive materials for investigating energy migration processes. Steady-state PL measurements by List et al. have demonstrated that in a solid-state blend of ladder type polyparaphenylene, mLPPP (host), and a molecular energy acceptor (guest), energy transfer occurs in a two-step process.[123] The first is thermally activated migration of the exciton within the donor polymer to a point sufficiently close to the acceptor that resonance energy transfer from the host to the guest can occur. The latter step is most often described in the framework of the Förster model.[29] This model is based on the weak coupling limit of radiationless transition theory, i.e., it is assumed that the energy transfer process occurs after vibrational relaxation in the donor excited state; in addition, the electronic coupling matrix element involved in the expression of the transfer rate is usually approximated using the point−dipole model. Recent time-resolved fluorescence data are consistent with dispersive relaxation dynamics of the photoexcitations in a polyfluorene film via incoherent hopping among localized states.[124]

In this section, our goal is first to review some recent experimental and theoretical work carried out to assess the relative rates of intrachain vs interchain exciton migration in luminescent conjugated poly-

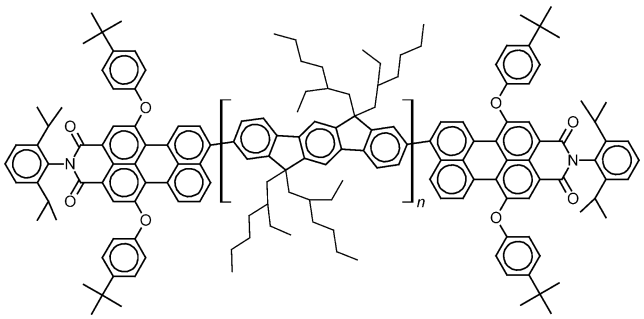

Figure 19. Molecular structure of α,ω-bis(N-(2,6-diisopropylphenyl)-1,6-bis(4-*tert*-butylphen oxy)-3,4-dicarbonicacidimide-9-perylene-poly-2,8-(6,6,12,12-tetraethylhexyl)-indenofluorene, PEC-PIFTEH.

mers.[114] The conjugated material investigated is a covalently linked donor−acceptor system, α,ω-bis(N-(2,6-diisopropylphenyl)-1,6-bis(4-*tert*-butylphenoxy)-3,4-dicarbonic-acidimide-9-perylene-poly-2,8(6,6, 12,-12-tetraethylhexyl)indenofluorene, hereafter abbreviated as PEC-PIFTEH (see the chemical structure in Figure 19). The molecules consist of red-emitting perylene monoimide (PEC) derivatives, covalently grafted at the ends of a blue-emitting derivative of polyindenofluorene (PIF). In solution, it is expected that incoherent exciton hopping along the PIF chains is the main energy migration channel. Because PEC-PIFTEH is a rigid system, in a good solvent such as *p*-xylene, no interactions due to chain folding should occur between the perylene end caps and the conjugated segments, in contrast to what is found in PPV derivatives.[122] Downhill exciton migration along the polymer chains toward low-energy sites is thus expected prior to energy transfer.[125] It is observed that intramolecular energy transfer rates in this polymer are slow as compared to the excited-state depopulation rate; in contrast, energy transfer is found to be very efficient in a solid film of the same material.

The exciton dynamics is interpreted in the framework of a theoretical approach based on an improved Förster model, wherein the electronic matrix elements for energy transfer are calculated from a multicentric atomic representation of the transition moments, i.e., under the form of atomic transition densities[126−129] and where both uphill and downhill jumps are treated on the same footing by considering the detailed donor emission and acceptor absorption spectra. This approach is briefly described in the next subsection. We have then successively considered the case of intramolecular energy transfer, where exciton transport takes place via hopping along the PIF chains followed by transfer to the perylene end caps, and intermolecular energy transfer simulated by considering two molecules in close contact; in both cases, the roles of geometric relaxation and local interactions between the atomic transition densities are highlighted.

5.1. Methodological Aspects

Because of their different chemical natures and the large torsion angle between the perylene derivative and the PIF chain, the two moieties in PEC-PIFTEH are decoupled as evidenced by the measured optical absorption spectrum of the polymer (which, to a good approximation, can be described as the superimposition of the PIFTEH and PEC absorptions[114]). We therefore investigated first the geometric and electronic structures of the individual units; we then assembled them to explore intrachain and interchain energy transfer processes. The ground-state (excited-state) geometries of a methyl-substituted PIF model chain and of the perylene derivative were optimized at the AM1 (AM1/CI) level assuming planar conformations. For the simulation of the intermolecular energy transfer, a complex formed by a perylene derivative lying on top of a PIF chain was optimized at the molecular mechanics level starting from a number of relative orientations; the intramolecular geometric parameters were frozen at the AM1 optimized values. A similar procedure was applied to model interchain migration between two neighbor indenofluorene segments.

The optimized geometries are then used as input for excited-state calculations (performed by means of the INDO/SCI formalism). The output of these calculations provides the excitation energies and transition dipole matrix elements from the ground state to the lowest excited states, as well as the corresponding atomic transition densities. For a transition from the ground state, ψ_g, to an excited state, ψ_e, of a molecule, the transition density on site m, $q(m)$, is written (within the zero-differential overlap approximation adopted here):

$$q^{g\rightarrow e}(m) = \sqrt{2}\Psi_e^*(m)\,\Psi_g(m) \qquad (27)$$

and can be related to the g → e transition dipole moment, $\mu_i^{g\rightarrow e}$, through

$$\mu_i^{g\rightarrow e} = \sum_m q^{g\rightarrow e}(m)\, r_i(m) \qquad (28)$$

where $r_i(m)$ denotes the atomic coordinates ($i \equiv x, y, z$) of site m and the summation is over all atomic sites (we recall that $\sum_m q^{g\rightarrow e}(m) = 0$ by virtue of orthogonality of the electronic states).

In Förster theory, the electronic coupling that promotes energy transfer from one molecule to another V_{DA} is usually calculated on the basis of a point−dipole model. Such an approach, which averages away the shapes of the donor and acceptor units, is applicable when the size of the molecules is small with respect to intermolecular separations. This condition is, however, hardly fulfilled in polymer materials, where the calculation of the long-range (dominant) Coulombic interactions should take into account the local shape of the wave functions.[130] Thus, one has turned to the distributed monopole method,[127−129] as developed for instance in the group of Markovitsi and Millié and the group of Fleming and Scholes. In that method, the total electronic coupling is estimated as the sum over atomic transition charges, thereby taking into account the spatial shape of the donor and acceptor via the transition densities of eq 27. The distributed monopole method

has been used here to calculate the electronic coupling V_{DA}:

$$V_{DA} = \sum_m \sum_n \frac{q_D(m)\, q_A(n)}{r_{mn}} \quad (29)$$

where the summations run over all sites m (n) on the donor (acceptor), r_{mn} denotes the distance between m and n, and $q_D(m)$ [$q_A(n)$] is the atomic transition density on site m (n) calculated for the lowest optical g → e excitation on the donor [acceptor].

Our aim here is to provide a qualitative description of intrachain vs interchain energy transfer in conjugated materials. Our analysis was based on a simple model that assumes that for the donor, energy is localized over one conformational subunit of the polymer chain. For the acceptor in an intrachain energy migration process, it is assumed that electronic interactions between neighboring acceptor conformational subunits are small enough that the acceptor density of states is not perturbed by electronic coupling between subunits. Admittedly, this can be a rather severe approximation for a quantitative treatment of intrachain energy migration;[131] however, in the linear chain model where there is no critical dependence on spectral overlap (e.g., the donor and acceptor densities of states are broad), this approximation allows one to provide an upper bound on the fastest intrachain energy transfer hopping rate.[132] With the transition rate, k_{DA}, expressed in ps^{-1} and the electronic coupling, V_{DA}, in cm^{-1}, we use eq 19 described in the Introduction for the donor-to-acceptor hopping rate:[21]

$$k_{DA} = 1.18|V_{DA}|^2 J_{DA} \quad (19)$$

where the overlap factors, J_{DA}, were calculated from (INDO/SCI) simulated absorption and emission spectra. The spectra were calculated within the displaced harmonic oscillator model, taking into account two vibrational modes:[133] a high-effective frequency mode (at 1300 cm^{-1}, corresponding to C−C stretching and ring breathing) accounting for the change in bond lengths when going from the ground state to the excited state and a low-frequency mode (at 80 cm^{-1}) coupled to the excitation due to the formation of a more planar excited-state geometry. Including the latter mode induces the emergence of a significant Stokes shift between absorption and emission and hence reduces the spectral overlap and energy transfer rate. Experimental investigations in phenylene-based materials also suggest that such a conformational geometric reorganization significantly slows down the exciton migration process.[134,135]

Although we do not describe it here (we only discuss simulations performed at room temperature), the temperature dependence of the excitation dynamics can be accounted for in this formalism through the homogeneous line widths and the resulting spectral overlap factors; these are indeed related to the population distribution in the vibrational manifold at a given temperature. Such a procedure provides a physical picture for dephasing effects governing the spectral homogeneous line widths in terms of either intrinsic (chromophore) or external (environment) low-frequency or "soft" vibrational modes. Note that the form of eq 19 accounts for the spectral inhomogeneity of the conformational subunit absorptions that are obscured within the broad polymer absorption band. Inhomogeneous broadening can thus be treated explicitly in these simulations by considering chromophores of different lengths and hence of different excitation energies. Because transition densities are used to calculate the electronic couplings, such an analysis differs significantly from the usual application of Förster theory to energy transfer involving conjugated polymers.

5.2. Singlet Energy Transfer in End-Capped PIF Chains

Experimental investigations on PEC-PIFTEH show that energy transfer is slow in solution and competes with the OIFs excited-state lifetimes, while several orders of magnitude faster in films where light emission only arises from the perylene acceptors.[114] Intrachain vs interchain exciton migration processes have been modeled in order to rationalize the difference in dynamics observed in solution and in films. From the experimental linear absorption spectrum, a ratio on the order of 50 is obtained for the PIFTEH over PEC contributions by integration of the solution optical spectrum. Because the oscillator strength calculated for one end-capped perylene derivative is similar to that of the individual repeat units in the PIF chains, an average polymer length on the order of 90−100 indenofluorene units is expected (since each polymer chain bears two perylene end groups and its oscillator strength scales linearly with the number, n, of monomers at large n). However, actual polymer lengths, estimated from gel permeation chromatography (GPC) data, are substantially smaller, on the order of ∼15 units.[114] One reason for this discrepancy, besides the inherent uncertainty related to GPC measurements on rigid-rod polymer chains, lies in the fact that a significant fraction of the polymer chains (as high as 50%) actually lack one or two perylene end groups. The simulations of long distance exciton transport have therefore been performed for polymer chains of increasing size (ranging from 10 to 100 repeat units).

The actual conjugation length, i.e., the length between two kinks along the conjugated path, has been estimated to lie in the range of 5−7 repeat units from extrapolation of the absorption and emission spectra of well-defined oligo(indenofluorenes) to those of the homopolymer.[136] Because the conjugation length is shorter than the real length of the PEC-PIFTEH chains, it is likely that excitation of one PIF segment in solution first induces exciton hopping along the main chain prior to energy transfer to the perylene end caps. In contrast, close contacts between indenofluorene segments and perylene end caps or among oligoindenofluorene (hereafter denoted as OIF) segments belonging to adjacent polymer chains should allow faster energy migration in the solid state.

To explore both intrachain and interchain transport channels, electronic couplings, spectral overlaps,

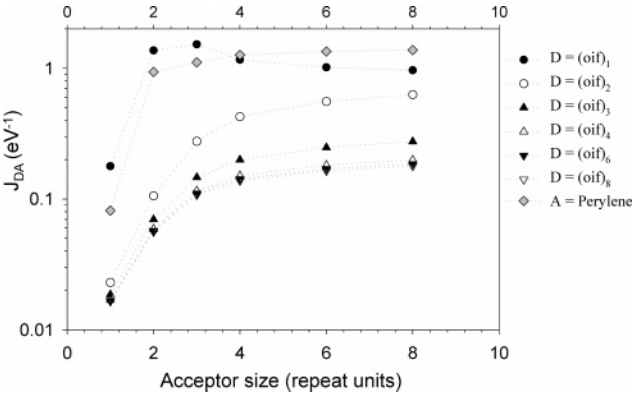

Figure 20. Spectral overlap factors computed for various OIF_n/OIF_m and OIF_n/PEC pairs on the basis of the simulated normalized donor emission and acceptor absorption spectra. Oligomers of indenofluorene with a conjugation length ranging from 1 to 8 units have been considered.

and single hopping transfer rates have been computed for a number of covalently linked donor−acceptor segments as well as donor−acceptor intermolecular stacks, considering indenofluorene oligomers ranging in size from one to eight repeat units. Spectral overlap factors computed for various OIF/OIF and OIF/PEC pairs on the basis of the simulated and measured normalized donor emission and acceptor absorption spectra are displayed in Figure 20 (these agree very well to experimental values estimated from the oligomer solution spectra[114]). When considering homomolecular transfer, the spectral overlap is calculated to increase with increasing acceptor size for a given donor size, while it decreases with increasing donor size for a given acceptor. Note that the spectral overlap factors computed in the case of heteromolecular transfer are found to be larger than the homomolecular counterparts, whatever the donor size. These evolutions stem from the subtle interplay between geometric relaxation energies ($E_{\mathrm{rel}}^{\mathrm{D}} \approx \lambda_i/2$) and shifts of the optical spectra due to changes in chromophore conjugation lengths Δ^{DA}. When the former exceeds the latter (as is the case here, except in the short oligomers), the spectral overlap is maximized for long acceptor chains and short donors, leading to the smallest mismatch between $E_{\mathrm{rel}}^{\mathrm{D}}$ and Δ^{DA}; see the scheme below.

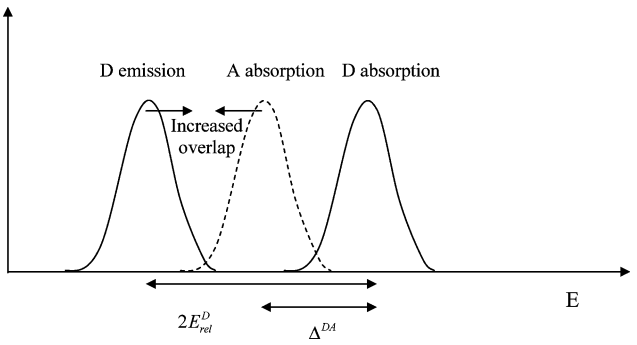

Comparison to spectral overlap factors calculated when neglecting low-frequency vibrational modes contributions suggests that flexible polymer chains should lead to less efficient intrachain energy migration than rigid rods, as a result of the relatively large relaxation energy associated to these soft modes and the concomitant reduced spectral overlap integrals.[133−135]

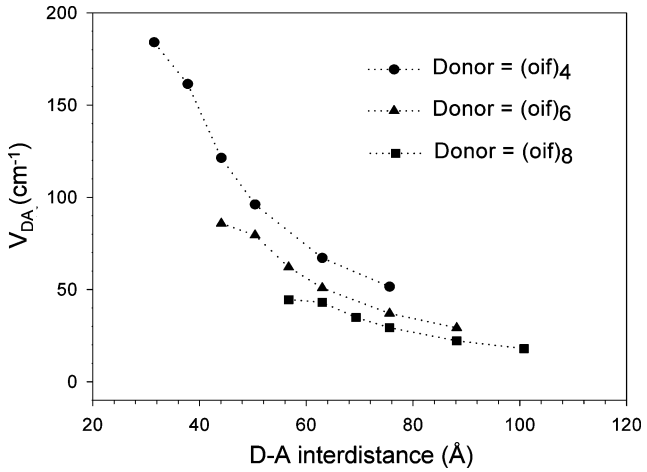

Figure 21. Electronic matrix elements, V_{DA}, for exciton hopping along the PIF backbone considering covalently linked OIF_n/OIF_m couples with varying donor and acceptor size.

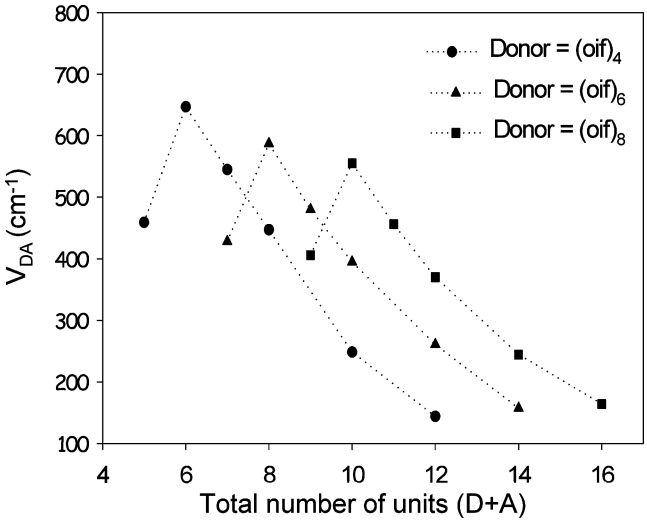

Figure 22. Same as for Figure 21 but for interchain energy transfer in cofacial dimers.

Electronic coupling matrix elements V_{DA} have been computed for both heteromolecular and homomolecular on-chain and interchain energy transfer using the distributed monopole model on the basis of relaxed excited-state geometries. The results are displayed in Figures 21 and 22 for intra- and interchain processes, respectively. When considering intrachain processes, electronic couplings computed for both homomolecular and heteromolecular (not shown) processes are found to drop quickly with the size of the donor and the acceptor. This arises from the increased intersite separations, together with a decrease in the transition density at the edges of the conformational subunits. In contrast, electronic matrix elements for interchain processes are maximized for an acceptor size of two indenofluorene units. In all cases, the V_{DA} values obtained for intermolecular transfer processes are found to be larger than their intrachain counterparts. It must be stressed that these results differ significantly from the predictions

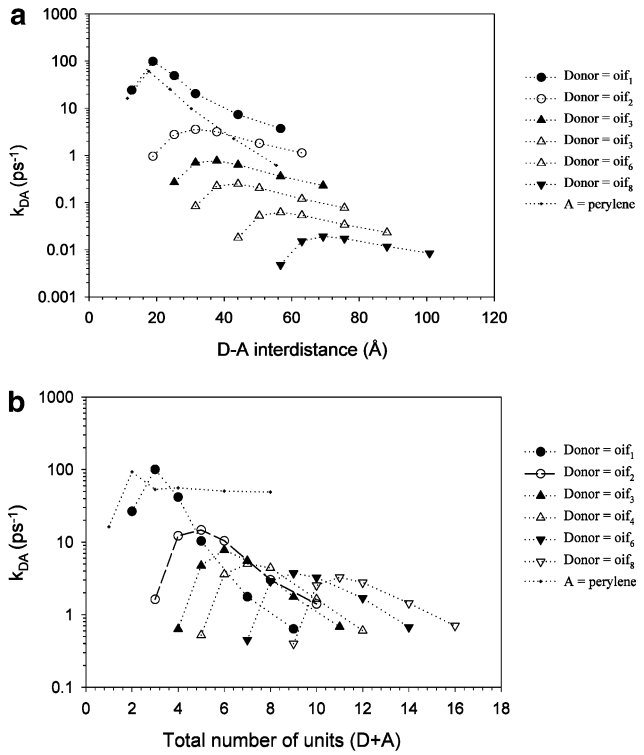

Figure 23. Intramolecular (a) and intermolecular (b) energy-transfer rates computed for different OIF_n/OIF_n and OIF_n/PEC donor−acceptor pairs differing by the size of the indenofluorene segments. Energy-transfer rates are plotted as a function of the donor plus acceptor conjugation lengths for cases where the donor is an indenofluorene dimer (circles), tetramer (up triangles), hexamer (solid down triangles), and octamer (down triangles).

of the widely used point−dipole approximation, both quantitatively and qualitatively.

Intermolecular and intramolecular energy hopping rates, as computed for different OIF donor−acceptor pairs, are displayed in Figure 23. Because the electronic couplings for both intrachain and interchain energy migration decrease with the size of the donor and the acceptor segments while the spectral overlap factors increase with acceptor size, the transfer rates for a given donor size are maximized for an intermediate acceptor length. Although similar trends are obtained for both processes, intermolecular rates are always larger than the corresponding on-chain values for given donor and acceptor sizes. Considering the tetramer as the donor, transfer rates for intrachain processes among indenofluorene oligomers range from 0.25 to 0.06 ps^{-1} depending on the acceptor size. The corresponding intermolecular transfer rates decrease from 3.3 to 0.7 ps^{-1} with donor/acceptor lengths. For heteromolecular transfer processes, the typical intrachain rates lie in the range 0.6−60 ps^{-1}; the corresponding interchain processes are found to be up to 1 order of magnitude faster with rates only weakly sensitive to chain length (in the range 50−90 ps^{-1}). These results suggest that a much more efficient energy transfer occurs in the solid state (where chain-to-chain contacts open new efficient channels) with respect to solution (assuming no direct contacts between the OIF segments and the perylene end caps), in good agreement with the faster dynamics observed experimentally in the solid state. The

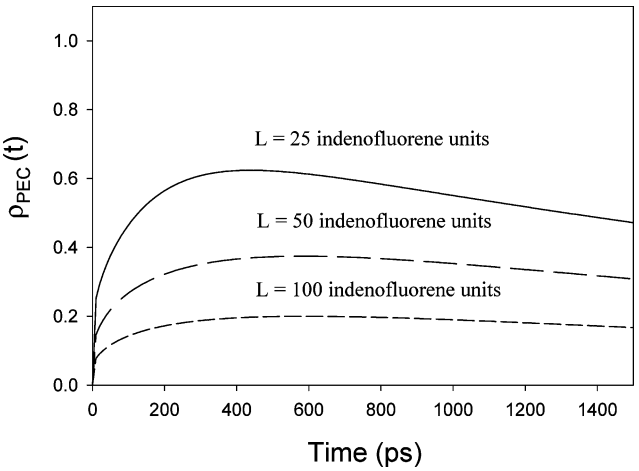

Figure 24. Time-dependent PIF population [$\rho_{PIF}(t)$] for a perylene end-capped linear polymer chain of total length 25, 50, and 100 repeat units. A distribution of oligomer lengths close to the experimental one (50% of hexamers and 25% of tetramers and octamers) has been adopted.

calculations also yield the correct order of magnitude for the interchain hopping rates (in the ps^{-1} range); a quantitative description is, however, difficult to achieve due to the sensitivity of the calculated electronic couplings on the relative donor−acceptor distance and separation.

It is also of interest to evaluate long-range intrachain energy migration. This has been modeled by solving the following Pauli Master equations (PME):

$$\frac{\partial}{\partial t} P_m(t) = -\sum_{n \neq m} [k_{mn} P_m(t) + P_m \tau_m^{-1} - k_{nm} P_n(t)] \quad (30)$$

where $P_m(t)$ denotes the time-dependent occupation probability on site m, k_{mn} is the rate for the excitation energy transfer from site m to site n as given by eq 19, and τ_m is the (radiative) lifetime for the excitation on the site m. The first term in the right-hand side of eq 30 describes the decay with time of $P_m(t)$ as a result of exciton migration from site m to all other sites; the third term is associated with the reverse hopping to site m from all sites $n \neq m$; the second term accounts for the natural exciton lifetime in absence of any transfer process (simply taken as the calculated radiative lifetime).

Equation 30 was applied to assess the excitation dynamics in PIF chains of 25, 50, and 100 indenofluorene units, built up from a statistical distribution of conjugated segments (50% hexamers, 25% tetramers, and 25% octamers). In the simulations, the populations $P_m(t)$ are equally distributed among all oligo(indenofluorene)s chromophores at time zero and then allowed to evolve with time according to the PME. As expected, the characteristic transient time to the perylene trap, defined here as the time at which the perylene population peaks, increases and the number of excitations that effectively reached the perylene group decreases with increasing chain length; see Figure 24. The characteristic time for the overall migration process is on the order of 800, 600, and

350 ps for chain lengths of 100, 50, and 25 units, respectively. The characteristic time values obtained for 25 and 50 repeat units are comparable to the calculated (radiative) donor excited-state lifetimes (which range from 600 to 400 ps in the more extended indenofluorene segments). A characteristic decay time of 500 ps has been extracted from the PIF-stimulated emission signal measured from time-resolved spectroscopy, which confirms that exciton hopping and decay occur on similar time scales.

The dynamics of exciton migration in the end-capped polymer chains can also be evaluated from the time evolution of the PL spectrum. Figure 25 shows emission spectra calculated for different time delays for lengths of 25, 50, and 100 indenofluorene units. The luminescence spectrum of the shortest chain (25 repeat units) is dominated by perylene emission for time delays larger than 500 ps, while almost equal contributions from perylene and the PIF chain are still obtained 1000 ps after excitation when considering a total chain length of 50 or 100 units. In the latter two cases, only excitations created close to the perylene end caps actually reach the acceptor chromophores, while a significant fraction of the photoinduced excited species decay radiatively on the PIF chain.

5.3. Extension to Annihilation Processes

Förster type resonance energy transfer is not restricted to energy transfer from an excited-state donor to a ground-state acceptor, as in the examples described above. It can also occur for instance from a chromophore in its first singlet excited state (S_1) to another chromophore either in its lowest triplet state (T_1) or lowest singlet excited state. All such processes are driven by long-range Coulombic interactions and differ only by the nature of the intervening electronic states; they can be described by the following reactions (A and B refer to two different chromophores):

$$\text{(i)}\ S_0^{A} + S_1^{B} \rightarrow S_1^{A} + S_0^{B}$$

$$\text{(ii)}\ S_1^{A} + S_1^{B} \rightarrow S_0^{A} + S_n^{B} \rightarrow S_0^{A} + S_1^{B} + \text{phonons}$$

$$\text{(iii)}\ S_1^{A} + T_1^{B} \rightarrow S_0^{A} + T_n^{B} \rightarrow S_0^{A} + T_1^{B} + \text{phonons}$$

where (i) corresponds to singlet hopping and (ii) and (iii) denote singlet−singlet and singlet−triplet annihilations, respectively; the second step in processes (ii) and (iii) corresponds to internal conversion down to the lowest singlet or triplet excited state.

In case (ii), two chromophores are excited almost simultaneously, which results in a bichromophore system where each of the chromophores is in the first singlet excited-state S_1. If the fluorescence of the chromophores is in resonance with a transition of S_1 to higher singlet excited states, i.e., a $S_1 \rightarrow S_n$ transition, energy transfer between the singlet excited states can occur. As the process results in only one excited state remaining in the bichromophoric system, it is often referred to as singlet−singlet annihilation. While this process is expected to play a minor role in LEDs due to the short singlet exciton lifetime and the moderate exciton densities, it could become crucial in the operation of organic lasers.

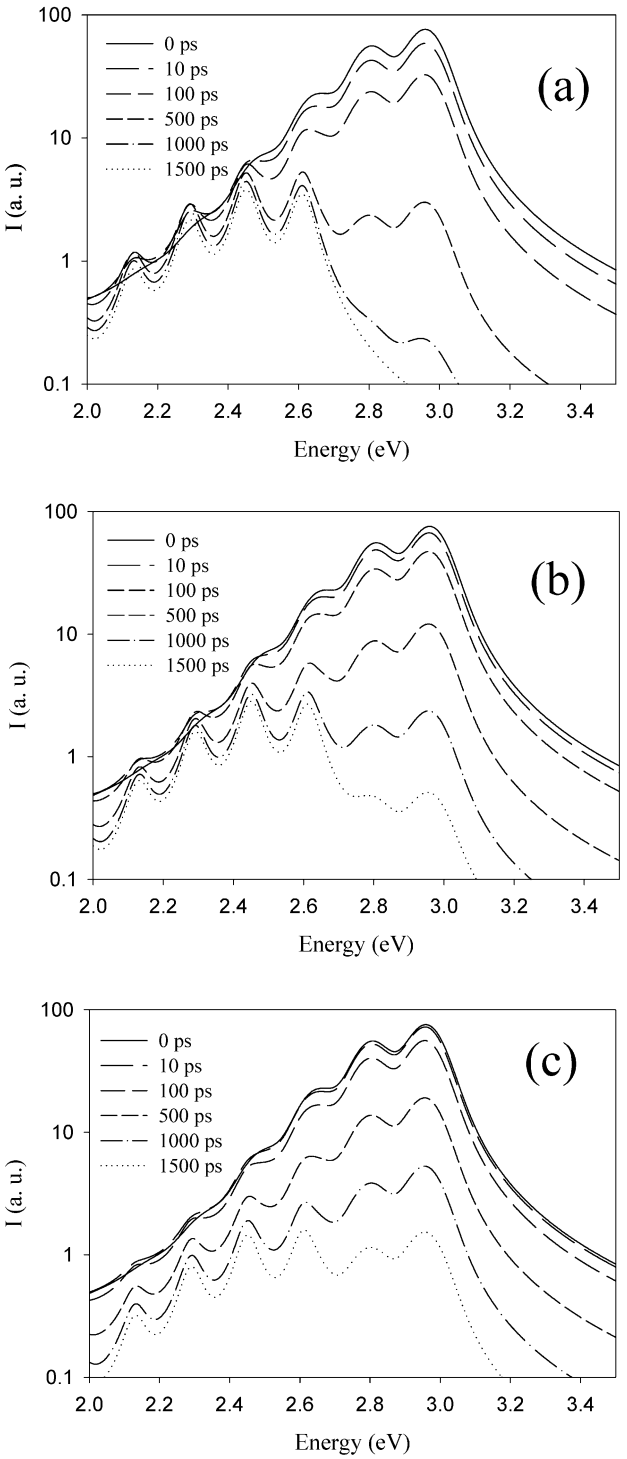

Figure 25. Time-dependent emission spectra for total chain lengths of 25 (a), 50 (b), and 100 repeat units (c).

Case (iii) involves intersystem crossing to a triplet state T_1 of chromophore B. When chromophore A is excited, again two excited states are present in the bichromophoric system: a singlet excited state (S_1) and a triplet excited state (T_1). If the triplet state is electronically coupled to higher-lying triplet excited states, T_n, that are in resonance with the $S_1 \rightarrow S_0$ transition, singlet−triplet energy transfer, i.e., energy transfer from the excited singlet state to the energetically lower-lying triplet state, can occur. This

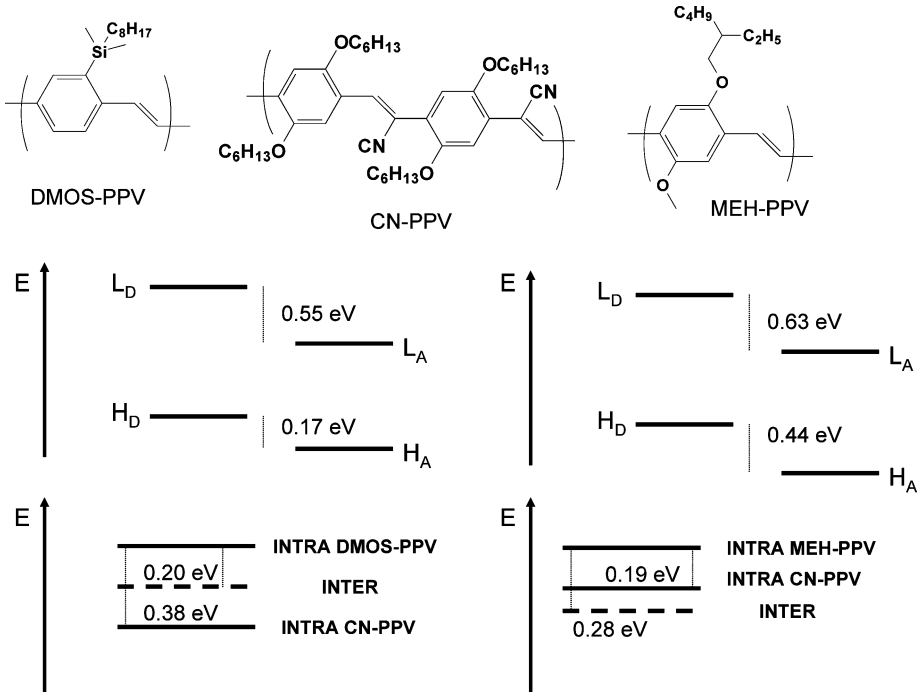

Figure 26. Description of the frontier electronic levels and ordering of the lowest intramolecular (INTRA) vs intermolecular (INTER) excited states in DMOS-PPV/CN-PPV and MEH-PPV/CN-PPV blends, as calculated at the INDO/SCI level.

process is often called singlet−triplet annihilation, as the net result is one excited state in the bichromoporic system, in this case a triplet state. Because the triplet populations in polymer LEDs can be high (as described in the previous section) and considering the long triplet lifetimes, it can be anticipated that such singlet−triplet collisions occur with a high probability; direct experimental evidence for singlet−triplet exciton annihilation in a ladder type polyphenylene has been reported by List et al.[137]

These competitive pathways have been explored in single bichromophoric systems consisting of peryleneimide end-capped fluorene oligomers, with chemical structures similar to that of PEC-PIFTEH in Figure 19. A similar methodology based on the weak coupling approximation and the improved Förster model was applied to evaluate the relative efficiencies of singlet energy hopping and singlet−singlet and singlet−triplet annihilations. To better account for electron correlation effects in the higher-lying singlet S_n and triplet T_n excited states, a multireference double configuration interaction formalism was applied to calculate the singlet−singlet and singlet−triplet atomic transition densities over the peryleneimide derivatives (here, the fluorene segment merely serves as a rigid spacer).

The calculated rates for the three processes in the bichromophoric systems were compared to the corresponding experimental values as determined from single-molecule spectroscopy investigations.[138] While the three processes are found to occur with similar efficiencies in the end-capped trimer molecule, annihilation processes turn out to be more efficient in longer oligomers due to better spectral overlaps; we note that the calculations underestimate the efficiency of singlet−triplet vs singlet−singlet annihilation. Further work will need to address these discrepancies as well as singlet-charge annihilation processes. The latter processes are indeed thought to be a major hurdle in the development of electrically driven organic lasers.[139]

6. Photoinduced Charge Separation in Organic Solar Cells

A critical step in the operation of a photovoltaic device is the charge separation of the excited electron−hole pair created upon photon absorption. This charge separation is triggered at the interface between a donor component and an acceptor component. An often-used description of the electronic structure of such a donor−acceptor blend, as shown in the central part of Figure 26, tends to imply that an off-set of the frontier electronic levels (HOMO and LUMO) of the donor and acceptor units is the major requirement to induce exciton dissociation. However, the situation is far from being that simple. Exciton dissociation can take place only if the energy gained by the electron (hole) when being transferred from the LUMO of the donor to the LUMO of the acceptor (from the HOMO of the acceptor to the HOMO of the donor) compensates for the binding energy of the intrachain exciton; thus, it is critical that the charge-separated state be the lowest excited state of the two-component system.

As demonstrated by Friend and co-workers,[140] polymer blends that display similar off-sets of their frontier electronic levels, as shown in Figure 26, can show very different charge-separation abilities. That work was concerned with the characterization of the electronic properties of two blends made of two different PPV-substituted derivatives, namely, a DMOS-PPV/CN-PPV blend and an MEH-PPV/CN-PPV blend; see the chemical structures in Figure 26 (note that the electronic structure of DMOS-PPV is nearly identical to that of PPV itself). According to

INDO calculations, there is a significant off-set between the frontier electronic levels of either DMOS-PPV or MEH-PPV (acting as donor) and those of CN-PPV (acting as acceptor); thus, efficient exciton dissociation might be expected in both blends. However, while experimental data demonstrate efficient charge generation in the MEH-PPV/CN-PPV blend, as evidenced by PL quenching and an increase in photocurrent, they point to energy transfer in the DMOS-PPV/CN-PPV blend, with a luminescence signal characteristic of the CN-PPV chains.[140]

Thus, these experimental observations cannot be explained by considering simply the HOMO and LUMO energies given in the middle of Figure 26. Their rationalization requires a model that takes into account the energies and ordering of the three relevant excited states: (i) the lowest intramolecular excited state of the donor (mainly described here by a donor HOMO−LUMO excitation); (ii) the lowest intramolecular excited state of the acceptor (originating similarly in an electron transition between its HOMO and LUMO levels); and (iii) the CT excited state resulting from electron excitation from HOMO to LUMO of the donor followed by ET to the LUMO of the acceptor. The bottom of Figure 26 provides the estimated ordering of these states in the two blends.

In going from DMOS-PPV to CN-PPV, the lowest intramolecular excited state is calculated to be red-shifted by 0.38 eV due to the asymmetric stabilization of the HOMO and LUMO levels in CN-PPV. The stabilization of the LUMO level by 0.55 eV induced by the cyano groups significantly lowers the energy of the lowest CT excited state; however, this stabilization is partly offset by the energy required to transform the intrachain exciton into an interchain exciton; the latter energy is not precisely known and has been taken to be around 0.35 eV. Therefore, the lowest CT excited state in the PPV/CN-PPV blend is estimated to be located some 0.20 eV below the lowest excited state of PPV and hence some 0.18 eV above the lowest intrachain excitation of CN-PPV. Thus, upon excitation of DMOS-PPV, what is expected to take place at the DMOS-PPV/CN-PPV interface is energy transfer toward the CN-PPV chains; this is supported by the experimental data.[140]

In the case of the MEH-PPV/CN-PPV pair, analysis of the one-electron structure indicates that the lowest optical transition of CN-PPV is red-shifted by 0.19 eV with respect to that of MEH-PPV while the LUMO level of CN-PPV is 0.63 eV lower than that of MEH-PPV. Taking into account that the stabilization of the lowest CT excited state has to incorporate the roughly 0.35 eV energy required to separate the electron and the hole, the lowest CT excited state in the MEH-PPV/CN-PPV blend is estimated to be ca. 0.28 eV (0.63−0.35) below the lowest intrachain transition of MEH-PPV; this is some 0.10 eV below the lowest excited state of CN-PPV. Thus, in this blend, the occurrence of a CT process is predicted at the polymer/polymer interface, in agreement with the experimental observations. Interestingly, these results demonstrate that a minor change in the substitution of the donor conjugated chains (the substitution involving either electroneutral silyl groups or electron-donating alkoxy groups) determines whether energy transfer or CT takes place to CN-PPV chains.

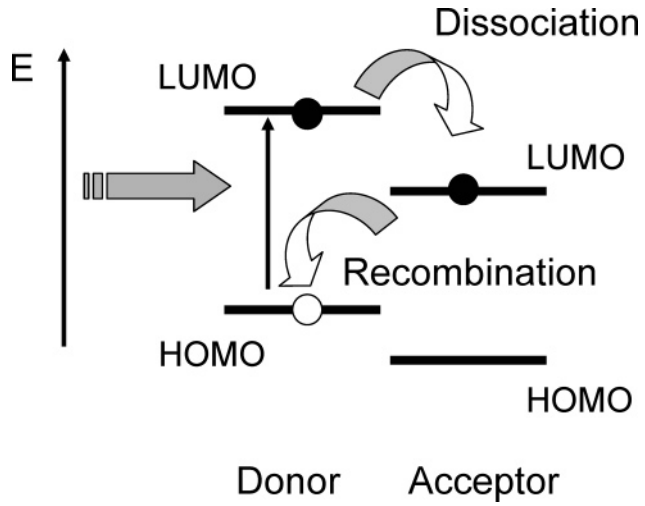

Figure 27. Illustration of the exciton dissociation and charge recombination processes in a donor/acceptor pair.

Although being instructive, the model outlined above suffers from strong limitations as the excitations are described in a one-electron picture and the exciton binding energy is introduced somewhat arbitrarily. As a result, it cannot be readily applied to any donor/acceptor pair. Moreover, it is critical to go beyond the static view based on the ordering of various excited states and to address the dynamics of the processes of importance in organic solar cells. Indeed, the exciton-dissociation process competes with a charge-recombination mechanism in which the charge-separated state decays back into the ground state of the blend (i.e., the electron in the LUMO level of the acceptor can transfer back to the HOMO level of the donor; see Figure 27); the back transfer mechanism should be as limited as possible to ensure efficient generation of charge carriers in the device.

It is interesting to note that much attention has been given to try and estimate theoretically the electronic couplings associated not only to photoinduced CT processes in donor−acceptor pairs or donor−bridge−acceptor architectures ($D^*BA \rightarrow D^+BA^-$) but also to CT processes occurring in the ground state (for instance of the kind $D^-BA \rightarrow DBA^-$).[52,141−143] Assuming within a one-electron picture that the excited state of the donor is described mainly by a HOMO−LUMO excitation and the CT excited state by a transition from the HOMO of the donor to the LUMO of the acceptor ($H_D \rightarrow L_A$), the electronic coupling for photoinduced CT can be considered to correspond to the transfer integral between the LUMO of the donor and that of the acceptor; this is similar to what happens in a ground-state $D^-BA \rightarrow DBA^-$ ET. Following Larsson and co-workers, the transfer integral can then be estimated as half the splitting of the LUMO levels obtained upon application of the electric field that creates a resonance between the two LUMO levels.[144−145]

However, it is desirable to go beyond such a one-electron picture and to introduce a CI description of the excited states. The electronic coupling can then be estimated as half the splitting of the intramolecu-

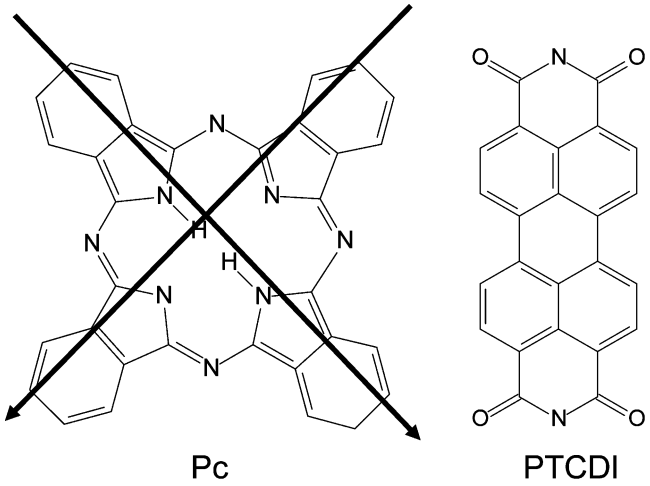

Figure 28. Chemical structures of Pc (left) and PTCDI (right); the arrows represent the orientation of the lowest two unoccupied orbitals of Pc.

lar and CT excited states at the transition state. Paddon-Row and co-workers have shown that the latter can be reached in a tractable way, when dealing with a limited number of configurations, by applying an electric field that equalizes the total amplitude of the CI coefficients describing the two states.[146]

The originality of the theoretical approach outlined below is to evaluate all terms entering the exciton dissociation and charge recombination rates at the correlated semiempirical quantum-chemical level.[147] To illustrate the basic aspects of this model, we have considered a donor/acceptor pair made of Pc as the donor and of perylene bisimide (PTCDI) as the acceptor (see the chemical structures in Figure 28). We note that blends of that nature are technologically relevant for organic solar cells and have been the subject of recent experimental studies;[148−149] Pc molecules are low-energy absorbers with the lowest absorption band peaking around 1.8 eV,[150] which closely matches the region where the solar emission is the most intense; PTCDI acceptors are becoming increasingly studied as an alternative to the widely used C_{60} derivatives.[151]

6.1. Evaluation of the Microscopic Parameters

Because exciton dissociation and charge recombination both correspond to an ET reaction, their rates have been estimated in the framework of the Bixon and Jortner model.[15] This formalism has been developed in the weak coupling limit; in the case of dissociation, this implies that the photoexcitation is initially localized on the donor (which has then time to relax to its optimal excited-state geometry); the subsequent ET yields a positive (negative) polaron localized on the donor (acceptor). Situations where the excitations and/or charges are delocalized over several molecules, as might occur in highly crystalline phases, are not considered here.

To describe photoinduced CT, the parameters ΔG^0, λ_i, λ_0, and V_{if} involved in eq 6 have been estimated as follows. The driving force ΔG^0 has been evaluated from Weller's equation[152] as the energy difference between the constituents in the final and initial states, taking account of the Coulomb attraction between the two polarons in the charge-separated state. In analogy to eqs 25 and 26 in section 4, ΔG^0 is written as:

$$\Delta G_{dis}{}^0 = E^{D+} + E^{A-} - E^{D^*} - E^{A} + E_{cb} \quad (31)$$

with

$$E_{cb} = \sum_D \sum_A \frac{q_D\, q_A}{\epsilon_s\, r_{DA}} \quad (32)$$

where E^{D^*}, E^{D+}, E^{A}, and E^{A-} represent the total energies of the donor in the equilibrium geometry of the lowest excited state and of the cationic state and those of the acceptor in the equilibrium geometry of the ground state and of the anionic state, respectively. The q_D and q_A terms correspond to the atomic charges on the donor and the acceptor, respectively (calculated at the AM1-CI/COSMO level following a Mulliken population analysis); r_{DA} is the distance separating the donor and the acceptor; and ϵ_s is the static dielectric constant of the medium. In the case of charge recombination, the donor and acceptor states become the charge-separated state and the ground state, respectively. In both cases, we have varied the static dielectric constant ϵ_s in the range 2.5−5, which is typical for organic thin films.[110]

The internal reorganization energy λ_i corresponds to the difference between the energy of the reactants (products) in the geometry characteristic of the products (reactants) and that of their equilibrium geometry. The two ways of estimating λ_i provide the same value only if the two parabolas representing the reactants and the products have the same curvature. Because this is often not the case, λ_i is usually estimated as the average of λ_{i1} and λ_{i2} defined for exciton dissociation as:

$$\lambda_{i1} = [E^{D^*}(Q_f) + E^{A}(Q_f)] - [E^{D^*}(Q_i) + E^{A}(Q_i)] \quad (33)$$

$$\lambda_{i2} = [E^{D+}(Q_i) + E^{A-}(Q_i)] - [E^{D+}(Q_f) + E^{A-}(Q_f)] \quad (34)$$

where Q_i and Q_f refer to the equilibrium geometry of the reactants and products, respectively.

The external reorganization energy λ_s has been estimated by the classical dielectric continuum model developed by Marcus.[118] Thus, the assumption is made here that the ET occurs in an isotropic dielectric environment, which is reasonable for amorphous blends. The reorganization term is given by:

$$\lambda_s = \frac{e^2}{2}\left(\frac{1}{\epsilon_{op}} - \frac{1}{\epsilon_s}\right)\left(\frac{1}{R_D} + \frac{1}{R_A} + 2\sum_D \sum_A \frac{q_D\, q_A}{r_{DA}}\right) \quad (35)$$

where e is the transferred electrical charge; ϵ_{op} denotes the optical dielectric constant of the medium (here set to a typical value of 2.25[153]); and R_D (= 4.06 Å) and R_A (= 3.45 Å) are the effective radii of the Pc and perylene molecules estimated from their total volume when assimilated to a sphere.

The electronic coupling V_{if} as it appears in eq 6 is to be evaluated in a diabatic description where the

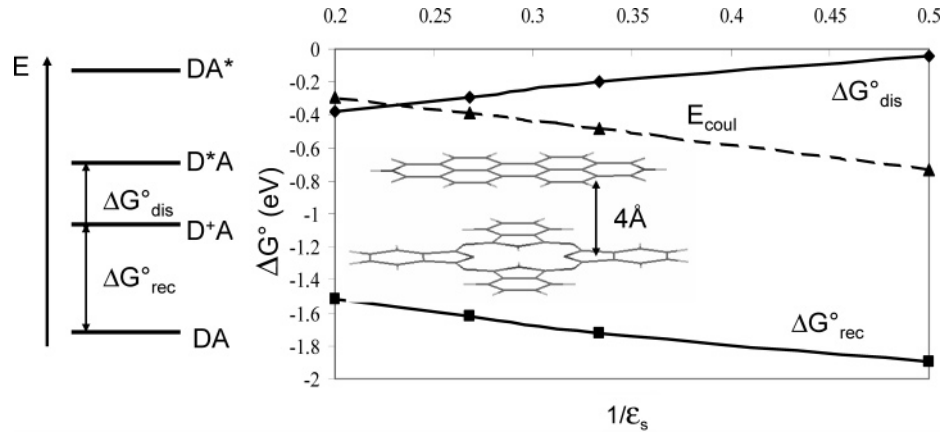

Figure 29. Evolution of $\Delta G°$ for exciton dissociation ($\Delta G_{dis}°$) and charge recombination ($\Delta G_{rec}°$) and of the Coulomb attraction between the polarons of opposite sign (E_{coul}) as a function of the inverse static dielectric constant ϵ_s in a Pc/PTCDI dimer (with the two molecules superimposed and separated by 4 Å), as calculated at the AM1-CI/COSMO level.

initial and final states do not interact. This is not the situation considered in the present correlated quantum-chemical calculations, which explicitly take into account the interaction between the two states, thereby providing an adiabatic description of the system. In this case, V_{if} can be estimated from the quantities given by CI calculations performed on the interacting donor/acceptor pair by using the generalized Mulliken−Hush formalism,[154−155] which refers to an optical process between the two states. V_{if} is then written as:

$$V_{if} = \frac{\mu_{if}\,\Delta E_{if}}{\sqrt{(\Delta\mu_{if})^2 + 4(\mu_{if})^2}} \qquad (36)$$

where ΔE_{if}, $\Delta\mu_{if}$, and μ_{if} correspond to the energy difference, the dipole moment difference, and the transition dipole moment between the initial and final states. This formalism is particularly attractive since it covers both photoinduced and ground-state CT processes and allows the inclusion of electron correlation in the description of the relevant states (the electronic coupling can also be estimated by plugging experimental values into eq 36).

In a first step, the parameters relevant for exciton dissociation have been calculated using the nuclear positions corresponding to the initial state by means of the INDO/SCI method, without any account of medium effects. We note that theoretical studies by Newton have confirmed the reliability of INDO with respect to ab initio calculations to estimate electronic couplings.[156] Because the calculated energy of the CT state is often not reliable due to the neglect of the intermolecular polarization effects, we have applied a static electric field along the CT direction to match ΔE_{if} to the $\Delta G_{dis}{}^0$ value provided by Weller's equation. This is clearly an approximation in the case of a vertical process where the energy of the CT state should be estimated in the geometry of the D*A (or DA*) state, considering the optical constant of the medium (thus, without the slow nuclear reorganization of the surrounding medium included in the static dielectric constant). However, this simple choice is relevant for charge recombination and is justified for exciton dissociation by the fact that the V_{if} amplitude is only weakly sensitive to changes in the actual energy of the CT state. In a second step, because the charge recombination starts from the fully equilibrated CT state, we have calculated to first approximation $\Delta\mu_{if}$ and μ_{if} in the D*A geometry with the same applied electric field. We then set ΔE_{if} equal to ΔG^0 for charge recombination to evaluate the electronic coupling using eq 36.

6.2. Pc–Perylenediimide Pair

We have considered a dimer made of a PTCDI molecule superimposed on a Pc molecule with a typical intermolecular distance of 4 Å. In Figure 29, the evolution of ΔG^0 is plotted for exciton dissociation ($\Delta G_{dis}{}^0$, assuming that the donor is initially excited) and charge recombination ($\Delta G_{rec}{}^0$) as a function of the inverse dielectric constant of the medium in the range between two and five. $\Delta G_{dis}{}^0$ is always negative, thus indicating that exciton dissociation occurs whatever the polarity of the medium. Its value becomes more negative (going from −0.20 eV at ϵ_s = 3 to −0.38 eV at ϵ_s = 5) when the dielectric constant is increased, even though the stabilizing Coulomb term is reduced by screening effects (from −0.48 eV at ϵ_s = 3 to −0.30 eV at ϵ_s = 5). Similar changes in the energy of the CT state upon variation of the medium polarity have been observed experimentally for ET reactions in solution.[157]

Analysis of the data indicates that exciton dissociation would be unfavorable or only weakly thermodynamically favored if the Coulomb attraction between the two polarons of opposite sign was neglected. Thus, it has to be realized that the two generated charges cannot easily escape their mutual attraction to yield free carriers (for instance, at room temperature, the two charges need to be separated by 11 nm in order to compensate for Coulomb attraction with ϵ_s = 5). It is clear that this Coulomb attraction is detrimental to the dissociation process required for the operation of the solar cells; in fact, many of the geminate polaron pairs (also referred to as exciplexes) decay either by nonradiative recombination or by light (exciplex) emission.[149,158,159] This raises the

important question of the nature of the mechanism allowing for the separation of the bound polaron pairs into free carriers. Several mechanisms have been proposed; for instance, Arkhipov et al. have highlighted the possible role of interfacial dipoles between the donor and the acceptor units in their ground state, which would facilitate the dissociation of the polaron pairs.[160] Janssen and co-workers have pointed to the possible role of disorder, which is intrinsic to organic thin films; in this view, the energy that the hole or the electron would gain by being transferred to a segment of lower energy would help to compensate for the Coulomb attraction.[161] Also, it has been proposed that the separation can be facilitated if it occurs prior to the thermalization of the polaron pairs, as noted by Bässler and co-workers and Conwell.[162,163]

Interestingly, the driving force for recombination ΔG_{rec}^0 becomes less negative when the polarity of the medium increases, as a result of the progressive stabilization of the charge-separated state. The calculated values for ΔG_{rec}^0 at $\epsilon_s = 3$ (−1.72 eV) and $\epsilon_s = 5$ (−1.52 eV) embrace the exciplex emission energy in Pc/PTCDI blends (1.63 eV),[149] which gives confidence in the reliability of the theoretical approach described above (we note, however, that a more accurate value of the exciplex emission should be calculated as the difference between the energy of the fully equilibrated D^+A^- state and that of the ground state in the D^+A^- geometry and polarized by the optical dielectric constant of the medium). The sum of ΔG_{rec}^0 and ΔG_{dis}^0 has an almost constant value (on the order of 1.9 eV, which is consistent with the energy of the lowest excited state of Pc), due to the fact that the energies of the ground state and the intramolecular excited states are only slightly affected by the medium polarity.

The internal reorganization energy λ_i is found to be slightly larger for the exciton dissociation (0.33 eV) than for the charge recombination (0.26 eV). The external reorganization energy λ_s has a similar order of magnitude and increases with the polarity of the medium (from 0.24 eV at $\epsilon_s = 3$ to 0.52 eV at $\epsilon_s = 5$), as expected. In the context of simple Marcus theory, since the sum of the two λ contributions is larger than $|\Delta G^0|$ for exciton dissociation, this process operates in the normal region of Marcus. In contrast, $|\Delta G^0|$ is larger than the total reorganization energy for charge recombination; thus, the latter is predicted to occur in the inverted region.

The electronic coupling V_{if} evolves from 447 to 445 cm^{-1} for exciton dissociation and from 1600 to 642 cm^{-1} for charge recombination when going from $\epsilon_s = 3$ to $\epsilon_s = 5$. That V_{if} is almost constant for exciton dissociation results from a compensation of the ΔE_{if} and μ_{if} terms in eq 36; this compensation does not occur for charge recombination. Note that these V_{if} values actually encompass two different pathways; this is the case because the lowest absorption band of Pc is made of two closely separated excited states that are mainly described by an electronic transition from the HOMO level to the LUMO or LUMO + 1 level, respectively (the lowest two unoccupied orbitals have very similar shapes and are oriented perpendicularly along the two branches of the conjugated core; see Figure 28).[150] We have thus defined V_{if} as the square root of the sum of the individual contributions ($V_{if1}^2 + V_{if2}^2$) of the two excited states, for which we have considered the same ΔG^0 and λ values.

All of the parameters discussed above can be entered into eq 6 to estimate the corresponding transfer rates. Doing so, we obtain values of 2.23×10^{13} and 1.20×10^{13} s^{-1} for the exciton-dissociation rate for $\epsilon_s = 3$ and 5, respectively. The transfer rate would increase if $|\Delta G^0|$ and λ_s were to converge toward a similar value; this does not occur here since the absolute value of both parameters increases with medium polarity. The reduction in transfer rate with ϵ_s is thus explained by the fact that the increase in λ_s is slightly larger than that in $|\Delta G^0|$. In contrast, charge recombination gets faster when the dielectric constant is increased (from 4.98×10^{11} to 4.79×10^{12} s^{-1} on going from $\epsilon_s = 3$ to 5). This is due to the opposite evolutions of $|\Delta G^0|$ and λ_s that reduce the gap between their absolute values. It is also of interest to analyze the evolution of the ratio k_{dis}/k_{rec} as a function of the dielectric constant; strikingly, the results indicate that this ratio goes from 45 at $\epsilon_s = 3$ to 2.5 at $\epsilon_s = 5$. Thus, an increase in the polarity of the medium leads to a situation where charge recombination increasingly competes with exciton dissociation.

These results demonstrate that the dielectric properties of the medium can play a key role in defining the efficiency of free carrier generation in organic solar cells. They also contrast with the usual understanding that exciton dissociation is much faster than charge recombination in donor/acceptor pairs; the latter case was found for instance in recent measurements on oligo(phenylenevinylene)-PTCDI copolymers that yield a k_{dis}/k_{rec} ratio on the order of a few hundreds.[164] The main difference is that we are dealing here with a Pc donor that presents a lowest excited state at much lower an energy than in oligo(phenylenevinylene)s, which results in a much lower $|\Delta G_{rec}^0|$. This is confirmed by the fact that the charge-recombination rate in the Pc/PTCDI blend for $\epsilon_s = 5$ is decreased by a factor of 40 or 3000 when $|\Delta G_{rec}^0|$ is increased artificially by 0.5 or 1 eV, respectively (which makes it go more deeply into the inverted Marcus regime).

We have also investigated the case where the acceptor is initially excited. The calculated dissociation rates lead to a ratio k_D/k_A [where k_D (k_A) corresponds to the rate when the donor (acceptor) is initially excited, respectively] of 45 and 6.3 for $\epsilon_s = 3$ and 5. The decrease in the exciton-dissociation rate when exciting the acceptor is associated with the increase in energy gap between $|\Delta G^0|$ and λ, the dissociation then taking place in the inverted region. Thus, the nature of the excited species also dictates the dynamics of charge generation in the device.

In conclusion of this section, we emphasize that the remarkable progress achieved recently in the field of organic photovoltaics has been more often than not the result of choosing donor and acceptor moieties on an empirical basis rather than on the basis of well-defined guidelines. Thus, the results of quantum-

chemical calculations such as those outlined in this section could provide materials chemists with new strategies for a rational design of donor−acceptor pairs.

7. Synopsis

The description of the electronic structure of π-conjugated materials has come a long way since the first calculations on polyenes and the attention given to the issues of bond length alternation and ordering of the lowest singlet excited states. After the discovery of highly conducting polymers, much of the interest focused on the evaluation of the ground-state properties (ionization potential, electron affinity, band gap, and bandwidths) and the evolution of the geometry and optical properties upon ionization (triggering the development of concepts such as solitons, polarons, and bipolarons).

In the mid-1980s, with the increased importance attached to nonlinear optical properties, the goal of many calculations was to determine the nature of the (unrelaxed) excited states playing a role in the second-order and third-order molecular polarizabilities. Relaxation effects in the excited states and impact of intermolecular interactions became the focus of numerous quantum-chemical studies in the 1990s due to the advent of electroluminescent conjugated polymers.

What we hope to have portrayed in this review is the increased significance of the dynamic processes taking place in π-conjugated materials, be them charge transport, charge recombination, exciton formation, exciton diffusion, or exciton dissociation. As a result, much attention is now devoted to the calculation of the rates for such energy-transfer or ET reactions, as they impact the characteristics of organic materials to be used in the new generations of electronic and photonic plastic devices.

8. Acknowledgments

We first acknowledge the essential contributions of several former and present group members to this review: in particular, M. Malagoli for section 2; J. P. Calbert, D. A. da Silva Filho, V. Lemaur, and O. Kwon for section 3; Z. Shuai and A. Ye for section 4; E. Hennebicq for section 5; and G. Pourtois for section 6. We also acknowledge fruitful collaborations and discussions with J. M. André, F. C. De Schryver, R. H. Friend, Y. Geerts, B. Kippelen, R. A. J. Janssen, R. Lazzaroni, S. R. Marder, M. A. Ratner, G. D. Scholes, R. Silbey, C. Silva, and E. Zojer. The work on π-conjugated materials at Georgia Tech has been partly supported by the National Science Foundation (through the STC Program under Award DMR-0120967, the MRSEC Program under Award DMR-0212302, and Grants CHE-0078819 and CHE-0342321), the Office of Naval Research, the Georgia Tech "Center on Organic Photonics and Electronics (COPE)", and the IBM Shared University Research Program; the work in Mons was supported by the Belgian Federal Government "InterUniversity Attraction Pole in Supramolecular Chemistry and Catalysis (PAI 5/3)" and "Technological Attraction Pole SOLTEX", the Région Wallonne (Program PIMENT-SOLPLAST), the European Commission project STEPLED (IST-2001-3735), and the Belgian National Fund for Scientific Research (FNRS). J.C. and D.B. are FNRS Research Fellows.

9. Note Added after ASAP Posting

This review was release ASAP on 9/28/2004. Equations 4 and 5 and the caption for Figure 3 were modified, and a clarifying phrase was added to the first paragraph in section 2. The review was reposted on 10/1/2004.

10. References

(1) Chiang, C. K.; Park, Y. W.; Heeger, A. J.; Shirakawa, H.; Louis, E. J.; MacDiarmid, A. G. *Phys. Rev. Lett.* **1977**, *39*, 1098.
(2) See, for instance: *Handbook of Conducting Polymers*, 2nd ed.; Skotheim, T. A., Reynolds, J. R., Elsenbaumer, R. L., Eds.; Marcel Dekker: New York, 1997.
(3) Tang, C. W.; VanSlyke, S. A. *Appl. Phys. Lett.* **1987**, *51*, 913.
(4) Burroughes, J. H.; Bradley, D. D. C.; Brown, A. R.; Marks, R. N.; Friend, R. H.; Burn, P. L.; Holmes, A. B. *Nature* **1990**, *347*, 539.
(5) Friend, R. H.; Gymer, R. W.; Holmes, A. B.; Burroughes, J. H.; Marks, R. N.; Taliani, C.; Bradley, D. D. C.; dos Santos, D. A.; Brédas, J. L.; Lögdlund, M.; Salaneck, W. R. *Nature* **1999**, *397*, 121.
(6) Sheats, J. R.; Antoniadis, H.; Hueschen, M.; Leonard, W.; Miller, J.; Moon, R.; Roitman, D.; Stocking, A. *Science* **1996**, *273*, 884.
(7) Sirringhaus, H.; Kawase, T.; Friend, R. H. *Science* **2000**, *290*, 2123.
(8) Baldo, M. A.; Thompson, M. E.; Forrest, S. R. *Nature* **2000**, *403*, 750.
(9) Grant, E.; Nolan, P.; Pinner, D. *McKinsey Q.* **2002**, *1*, 18.
(10) Horowitz, G. *Adv. Mater.* **1998**, *10*, 365.
(11) Huitema, H. E. A.; Gelinck, G. H.; van der Putten, J. B. P. H.; Kuijk, K. E.; Hart, K. M.; Cantatore, E.; de Leeuw, D. M. *Adv. Mater.* **2002**, *14*, 1201.
(12) (a) Halls, J. J. M.; Walsh, C. A.; Greenham, N. C.; Marseglia, E. A.; Friend, R. H.; Moratti, S. C.; Holmes, A. B. *Nature* **1995**, *376*, 498. (b) Brabec, C. J.; Sariciftci, N. S.; Hummelen, J. C. *Adv. Funct. Mater.* **2001**, *11*, 15.
(13) (a) Zhou, Q.; Swager, T. M. *J. Am. Chem. Soc.* **1995**, *117*, 12593. (b) McQuade, D. T.; Pullen, A. E.; Swager, T. M. *Chem. Rev.* **2000**, *100*, 2537. (c) McQuade, D. T.; Hegedus, A. H.; Swager, T. M. *J. Am. Chem. Soc.* **2000**, *122*, 12389.
(14) *Electron Transfer in Chemistry*; Balzani, V., Ed.; Wiley-VCH: Weinheim, 2001.
(15) *Electron Transfer: From Isolated Molecules to Biomolecules, Adv. Chem. Phys.*; Bixon, M., Jortner, J., Eds.; Wiley: New York, 1999; Vols. 106−107.
(16) (a) Marcus, R. A. *Rev. Mod. Phys.* **1993**, *65*, 599. (b) Marcus, R. A. *J. Chem. Phys.* **1956**, *24*, 966 and 979. (c) Marcus, R. A.; Sutin, N. *Biochim. Biophys. Acta* **1985**, *811*, 265.
(17) Reimers, J. R. *J. Chem. Phys.* **2001**, *115*, 9103.
(18) Silinsh, E. A.; Klimkans, A.; Larsson, S.; Capek, V. *Chem. Phys.* **1995**, *198*, 311.
(19) Pope, M.; Swenberg, C. E. *Electronic Processes in Organic Crystals and Polymers*, 2nd ed.; Oxford University Press: New York, 1999.
(20) Malagoli, M.; Brédas, J. L. *Chem. Phys. Lett.* **2000**, *327*, 13.
(21) *Charge and Energy Transfer Dynamics in Molecular Systems*; May, V., Kühn, O., Eds.; Wiley-VCH: Berlin, 2000.
(22) Wilson, E. B.; Decius, J. C.; Cross, P. C. *Molecular Vibrations*; Dover: New York, 1980.
(23) Köppel, H.; Domcke, W.; Cederbaum, L. S. *Adv. Chem. Phys.* **1984**, *57*, 59.
(24) Devos, A.; Lannoo, M. *Phys. Rev. B* **1998**, *58*, 8236.
(25) (a) Kato, T.; Yamabe, T. J. *J. Chem. Phys.* **2001**, *115*, 8592. (b) Kato, T.; Yamabe, T. J. *J. Chem. Phys.* **2002**, *117*, 2324. (c) Kato, T.; Yamabe, T. J. *J. Chem. Phys.* **2003**, *118*, 3300. (d) Kato, T.; Yamabe, T. J. *J. Chem. Phys.* **2004**, *120*, 3311. (e) Kato, T.; Yamabe, T. J. *J. Chem. Phys.* **2004**, *120*, 1006.
(26) Koopmans, T. *Physica* **1933**, *1*, 104.
(27) Duschinsky, F. *Acta Physicochim. URSS* **1937**, *7*, 551.
(28) Wong, K. Y.; Schatz, P. N. *Prog. Inorg. Chem.* **1981**, *28*, 369.
(29) Förster, Th. *Ann. Phys.* **1948**, *2*, 55.
(30) Chen, P. *Unimolecular and Bimolecular Ion−Molecule Reaction Dynamics*; Ng, C.-Y., Baer, T., Powis, I., Eds.; John Wiley & Sons: New York, 1994; pp 372−425.

(31) Mok, D. K. W.; Lee, E. P. F.; Chau, F. T.; Wang, D. C.; Dyke, J. M. *J. Chem. Phys.* **2000**, *113*, 5791.
(32) Sando, G. M.; Spears, K. G. *J. Phys. Chem. A* **2001**, *105*, 5326.
(33) Kupka, H.; Cribb, P. H. *J. Chem. Phys.* **1986**, *85*, 1303.
(34) Schumm, S.; Gerhards, M.; Kleinermanns, K. *J. Phys. Chem. A* **2000**, *104*, 10648.
(35) Ballhausen, C. J. *Molecular Electronic Structures of Transition Metal Complexes*; McGraw-Hill: New York, 1979.
(36) (a) Gruhn, N. E.; da Silva Filho, D. A.; Bill, T. G.; Malagoli, M.; Coropceanu, V.; Kahn, A.; Brédas, J. L. *J. Am. Chem. Soc.* **2002**, *124*, 7918. (b) Coropceanu, V.; Malagoli, M.; da Silva Filho, D. A.; Gruhn, N. E.; Bill, T. G.; Brédas, J. L. *Phys. Rev. Lett.* **2002**, *89*, 275503. (c) Coropceanu, V.; Andre, J. M.; Malagoli, M.; Brédas, J. L. *Theor. Chem. Acc.* **2003**, *110*, 59.
(37) (a) Malagoli, M.; Coropceanu, V.; da Silva Filho, D. A.; Brédas, J. L. *J. Chem. Phys.* **2004**, *120*, 7490. (b) da Silva Filho, D. A.; Friedlein, R.; Coropceanu, V.; Öhrwall, G.; Osikowicz, W.; Suess, C.; Sorensen, S. L.; Svensson, S.; Salaneck, W. R.; Brédas, J. L. *Chem. Commun.* **2004**, 1702. (c) Kwon, O.; Coropceanu, V.; Gruhn, N. E.; Durivage, J. C.; Laquindanum, J. G.; Katz, H. E.; Cornil, J.; Brédas, J. L. *J. Chem. Phys.* **2004**, *120*, 8186.
(38) Nelson, S. F.; Lin, Y. Y.; Gundlach, D. J.; Jackson, T. N. *Appl. Phys. Lett.* **1998**, *72*, 1854.
(39) Sundar, V. C.; Zaumseil, J.; Podzorov, V.; Menard, E.; Willett, R. L.; Someya, T.; Gersherson, M. E.; Rogers, J. A. *Science* **2004**, *303*, 1644.
(40) Klimkans A.; Larsson, S. *Chem. Phys.* **1994**, *189*, 25.
(41) Wong, W. *Chem. Phys. Lett.* **1996**, *256*, 391.
(42) Anthony, J. E.; Brooks, J. S.; Eaton, D. L.; Parkin, S. R. *J. Am. Chem. Soc.* **2001**, *123*, 9482.
(43) Meng, H.; Bendikov, M.; Mitchell, G.; Helgeson, R.; Wudl, F.; Bao, Z.; Siegrist, T.; Kloc, C.; Chen, C. H. *Adv. Mater.* **2003**, *15*, 1090.
(44) Cornil, J.; Lemaur, V.; Steel, M. C.; Dupin, H.; Burquel, A.; Beljonne, D.; Brédas, J. L. In *Organic Photovoltaic: Mechanisms, Materials and Devices*; Sun, S., Sariciftci, N. S., Eds.; Marcel Dekker: New York, in press.
(45) Lemaur, V.; da Silva Filho, D. A.; Coropceanu, V.; Lehmann, M.; Geerts, Y.; Piris, J.; Debije, M. G.; van de Craats, A. M.; Senthilkumar, K.; Siebbeles, L. D. A.; Warman, J. M.; Brédas, J. L.; Cornil, J. *J. Am. Chem. Soc.* **2004**, *126*, 3271.
(46) Fichou, D. *J. Mater. Chem.* **2000**, *10*, 571.
(47) Duke, C. B.; Schein, L. B. *Phys. Today* **1980**, *February*, 42.
(48) Warta, W.; Stehle, R.; Karl, N. *Appl. Phys. A* **1985**, *36*, 163.
(49) Jurchescu, O. D.; Baas, T.; Palstra, T. T. M. *Appl. Phys. Lett.* **2004**, *84*, 3061.
(50) Wu, M. W.; Conwell, E. M. *Chem. Phys. Lett.* **1997**, *266*, 363.
(51) (a) Brédas, J. L.; Calbert, J. P.; da Silva Filho, D. A.; Cornil, J. *Proc. Natl. Acad. Sci. U.S.A.* **2002**, *99*, 5804. (b) Cornil, J.; Beljonne, D.; Calbert, J. P.; Brédas, J. L. *Adv. Mater.* **2001**, *13*, 1053.
(52) Newton, M. D. *Chem. Rev.* **1991**, *91*, 767.
(53) (a) Li, X. Y.; Tang, X. S.; He, F. C. *Chem. Phys.* **1999**, *248*, 137. (b) Li, X. Y.; He, F. C. *J. Comput. Chem.* **1999**, *20*, 597.
(54) Pati, R.; Karna, S. P. *J. Chem. Phys.* **2001**, *115*, 1703.
(55) Wolfsberg, M.; Helmhotz, L. *J. Chem. Phys.* **1952**, *20*, 837.
(56) Pietro, W. J.; Marks, T. J.; Ratner, M. A. *J. Am. Chem. Soc.* **1985**, *107*, 5387.
(57) Liang, C.; Newton, M. D. *J. Phys. Chem.* **1992**, *96*, 2855.
(58) Paulson, B. P.; Curtiss, L. A.; Bal, B.; Closs, G. L.; Miller, J. R. *J. Am. Chem. Soc.* **1996**, *118*, 378.
(59) Voityuk, A. A.; Rösch, N.; Bixon, M.; Jortner, J. *J. Phys. Chem. B* **2000**, *104*, 9740.
(60) Grozema, F. C.; van Duijnen, P. T.; Berlin, Y. A.; Ratner, M. A.; Siebbeles, L. D. A. *J. Phys. Chem. B* **2002**, *106*, 7791.
(61) Palenberg, M. A.; Silbey, R. J.; Malagoli, M.; Brédas, J. L. *J. Chem. Phys.* **2000**, *112*, 1541.
(62) Senthilkumar, K.; Grozema, F. C.; Bickelhaupt, F. M.; Siebbeles, L. D. A. *J. Chem. Phys.* **2003**, *119*, 9809.
(63) Mattheus, C. C. Polymorphism and Electronic Properties of Pentacene, Ph.D. Thesis, University of Groningen, The Netherlands, 2002.
(64) Adam, D.; Schuhmacher, P.; Simmerer, J.; Häussling, L.; Siemensmeyer, K.; Etzbach, K. H.; Ringsdorf, H.; Haarer, D. *Nature* **1994**, *371*, 141.
(65) Cornil, J.; Lemaur, V.; Calbert, J. P.; Brédas, J. L. *Adv. Mater.* **2002**, *14*, 726.
(66) Watson, M. D.; Fechtenkötter, A.; Müllen, K. *Chem. Rev.* **2001**, *101*, 1267.
(67) Lehmann, M.; Lemaur, V.; Cornil, J.; Brédas, J. L.; Goddard, S.; Grizzi, I.; Geerts, Y. *Tetrahedron* **2004**, *60*, 3283.
(68) Horowitz, G.; Bachet, B.; Yassar, A.; Lang, P.; Demanze, F.; Fave, J. L.; Garnier, F. *Chem. Mater.* **1995**, *7*, 1337.
(69) Siegrist, T.; Fleming, R. M.; Haddon, R. C.; Laudise, R. A.; Lovinger, A. J.; Katz, H. E.; Bridenbaugh, P.; Davis, D. D. *J. Mater. Res.* **1995**, *10*, 2170.
(70) Ponomarev, V. I.; Filipenko, O. S.; Atovmyan, L. O. *Kristallografiya* **1976**, *21*, 392.
(71) Brock C. P.; Dunitz, J. D. *Acta Crystallogr. Sect. B: Struct. Sci.* **1990**, *46*, 795.
(72) Holmes, D.; Kumaraswamy, S.; Matzger, A. J.; Vollhardt, K. P. C. *Chem. Eur. J.* **1999**, *5*, 3399.
(73) Mattheus, C. C.; de Wijs, G. A.; de Groot, R. A.; Palstra, T. T. M. *J. Am. Chem. Soc.* **2003**, *125*, 6323.
(74) Li, X. C.; Sirringhaus, H.; Garnier, F.; Holmes, A. B.; Moratti, S. C.; Feeder, N.; Clegg, W.; Teat, S. J.; Friend, R. H. *J. Am. Chem. Soc.* **1998**, *120*, 2206.
(75) Cheng, Y. C.; Silbey, R. S.; da Silva Filho, D. A.; Calbert, J. P.; Cornil, J.; Brédas, J. L. *J. Chem. Phys.* **2003**, *118*, 3764.
(76) Horowitz, G. *Adv. Mater.* **1998**, *10*, 365.
(77) Schoonveld, W. A.; Vrijmoeth, J.; Klapwijk, T. M. *Appl. Phys. Lett.* **1998**, *73*, 3884.
(78) Torsi, L.; Dodabalapur, A.; Rothberg, L. J.; Fung, A. W. P.; Katz, H. E. *Phys. Rev. B* **1998**, *57*, 2271.
(79) Haddon, R. C.; Siegrist, T.; Fleming, R. M.; Bridenbaugh, P. M.; Laudise, R. A. *J. Mater. Chem.* **1995**, *5*, 1719.
(80) Siegrist, T.; Kloc, C.; Laudise, R. A.; Katz, H. E.; Haddon, R. C. *Adv. Mater.* **1998**, *10*, 379.
(81) Widany, J.; Daminelli, G.; Di Carlo, A.; Lugli, P.; Jungnickel, G.; Elstner, M.; Frauenheim, Th. *Phys. Rev. B* **2001**, *63*, 233204.
(82) Puschnig, P.; Ambrosch-Draxl, C. *Phys. Rev. B* **1999**, *60*, 7891.
(83) (a) Tiago, M. L.; Northrup, J. E.; Louie, S. G. *Phys. Rev. B* **2003**, *67*, 115212. (b) Haddon, R. C.; Chi, X.; Itkis, M. E.; Anthony, J. E.; Eaton, D. L.; Siegrist, T.; Mattheus, C. C.; Palstra, T. T. M. *J. Phys. Chem. B* **2002**, *106*, 8288.
(84) (a) Hannewald, K.; Bobbert, P. A. *Phys. Rev. B* **2004**, *69*, 075212. (b) Stojanovic, V. M.; Bobbert, P. A.; Michels, M. A. J. *Phys. Rev. B* **2004**, *69*, 144302. (c) Masino, M.; Girlando, A.; Brillante, A.; Farina, L.; Della Valle, R. G.; Venuti, E. *Macromol. Symp.* **2004**, *212*, 375. (d) Girlando, A.; Masino, M.; Brillante, A.; Della Valle, R. G.; Venuti, E. *Phys. Rev. B* **2002**, *66*, 100507. (e) Sinova, J.; Schliemann, J.; Nunez, A. S.; MacDonald, A. H. *Phys. Rev. Lett.* **2001**, *87*, 226802. (f) Bussac, M. N.; Picon, J. D.; Zuppiroli, L. *Europhys. Lett.* **2004**, *66*, 392.
(85) *Primary Photoexcitations in Conjugated Polymers: Molecular Exciton versus Semiconductor Band Model*; Sariciftci, N. S., Ed.; World Scientific: Singapore, 1997.
(86) Chawdhury, N.; Köhler, A.; Friend, R. H.; Wong, W.-Y.; Lewis, J.; Younus, M.; Raithby, P. R.; Corcoran, T. C.; Al-Mandhary, M. R. A.; Kahn, M. S. *J. Chem. Phys.* **1999**, *110*, 4963.
(87) Köhler, A.; Wilson, J. S.; Friend, R. H.; Al-Suti, M. K.; Khan, M. S.; Gerhard, A.; Bässler, H. *J. Chem. Phys.* **2002**, *116*, 9457.
(88) Monkman, A. P.; Burrows, H. D.; Hartwell, L. J.; Horsburgh, L. E.; Hamblett, I.; Navaratnam, S. *Phys. Rev. Lett.* **2001**, *86*, 1358.
(89) Romanvskii, Y. V.; Gerhard, A.; Schweitzer, B.; Scherf, U.; Personov, R. I.; Bässler, H. *Phys. Rev. Lett.* **2000**, *84*, 1027.
(90) Hertel, D.; Setayesh, S.; Nothofer, H. G.; Scherf, U.; Personov, R. I.; Bässler, H. *Adv. Mater.* **2001**, *13*, 65.
(91) Beljonne, D.; Shuai, Z.; Friend, R. H.; Brédas, J. L. *J. Chem. Phys.* **1995**, *102*, 2042.
(92) Segal, M.; Baldo, M. A.; Holmes, R. J.; Forrest, S. R.; Soos, Z. G. *Phys. Rev. B* **2003**, *68*, 075211.
(93) Cao, Y.; Parker, I. D.; Yu, G.; Zhang, C.; Heeger, A. J. *Nature* **1999**, *397*, 414.
(94) (a) Ho, P. K. H.; Kim, J.; Burroughes, J. H.; Becker, H.; Li, S. F. Y.; Brown, T. M.; Cacialli, F.; Friend, R. H. *Nature* **2000**, *404*, 481. (b) Wilson, J. S.; Dhoot, A. S.; Seeley, A. J. A. B.; Khan, M. S.; Köhler, A.; Friend, R. H. *Nature* **2001**, *413*, 828.
(95) (a) Wohlgenannt, M.; Tandon, K.; Mazumdar, S.; Ramasesha, S.; Vardeny, Z. V. *Nature* **2001**, *409*, 494. (b) Wohlgenannt, M.; Jiang, X. M.; Vardeny, Z. V.; Janssen, R. A. J. *Phys. Rev. Lett.* **2002**, *88*, 197401.
(96) Dhoot, A. S.; Ginger, D. S.; Beljonne, D.; Shuai, Z.; Greenham, N. C. *Chem. Phys. Lett.* **2002**, *360*, 195.
(97) Virgili, T.; Cerullo, G.; Lüer, L.; Lanzani, G.; Gadermaier, C.; Bradley, D. D. C. *Phys. Rev. Lett.* **2003**, *90*, 247402.
(98) Meulenkamp, E. A.; van Aar, R.; Bastiaansen, J. J. A. M.; van den Biggelaar, A. J. M.; Börner, H.; Brunner, K.; Büchel, M.; van Dijken, A.; Kiggen, N. M. M.; Kilitziraki, M.; de Kok, M. M.; Langeveld, B. M. W.; Ligter, M. P. H.; Vulto, S. I. E.; van de Weijer, P.; de Winter, S. H. P. M. *SPIE-Int. Soc. Opt. Eng.* In press.
(99) Shuai, Z.; Beljonne, D.; Silbey, R. J.; Brédas, J. L. *Phys. Rev. Lett.* **2000**, *84*, 131.
(100) Kobrak, M. N.; Bittner, E. R. *Phys. Rev. B* **2000**, *62*, 11473.
(101) Karabunarliev, S.; Bittner, E. R. *Phys. Rev. Lett.* **2003**, *90*, 057402.
(102) Tandon, K.; Ramasesha, S.; Mazumdar, S. *Phys. Rev. B* **2003**, *67*, 045109.
(103) Hong, T.; Meng, H. *Phys. Rev. B* **2003**, *63*, 075206.
(104) Baldo, M. A.; O'Brien, D. F.; Thompson, M. E.; Forrest, S. R. *Phys. Rev. B* **1999**, *60*, 14422.
(105) Frankevich, E. L.; Lymarev, A. A.; Sokolik, I.; Karasz, F. E.; Blumstengel, S.; Baughman, R. H.; Hörhold, H. H. *Phys. Rev. B* **1992**, *46*, 9329.
(106) Dyakonov, V.; Rösler, G.; Schwoerer, M.; Frankevich, E. L. *Phys. Rev. B* **1997**, *56*, 3852.

(107) Kadashchuk, A.; Vakhnin, A.; Blonski, I.; Beljonne, D.; Shuai, Z.; Brédas, J. L.; Arkhipov, V. I.; Heremans, P.; Emelianova, E. V.; Bässler, H. *Phys. Rev. Lett*. **2004**, *93*, 066803.
(108) Beljonne, D.; Ye, A.; Shuai, Z.; Brédas, J. L. *Adv. Funct. Mater.* **2004**, *14*, 684.
(109) (a) Klamt, A.; Schürmann, G. *J. Chem. Soc., Perkin Trans.* **1993**, *2*, 799. (b) Tomasi, J.; Persico, M. *Chem. Rev.* **1994**, *94*, 2027.
(110) Comoretto, D.; Dellepiane, G.; Marabelli, F.; Cornil, J.; dos Santos, D. A.; Brédas, J. L.; Moses, D. *Phys. Rev. B* **2000**, *62*, 10173.
(111) van der Horst, J. W.; Bobbert, P. A.; de Jong, P. H. L.; Michels, M. A. J.; Brocks, G.; Kelly, P. J. *Phys. Rev. B* **2000**, *61*, 15817. According to these authors, it is the perpendicular dielectric constant that plays the dominant role in the interchain screening along the chain; a value of ~3 was calculated for that component.
(112) Cornil, J.; Beljonne, D.; Friend, R. H.; Brédas, J. L. *Chem. Phys. Lett.* **1994**, *223*, 82.
(113) Chandross, M.; Mazumdar, S.; Liess, M.; Lane, P. A.; Vardeny, Z. V.; Hamaguchi, M.; Yoshino, K. *Phys. Rev. B* **1997**, *55*, 1486.
(114) (a) Beljonne, D.; Pourtois, G.; Silva, C.; Hennebicq, E.; Herz, L. M.; Friend, R. H.; Scholes, G. D.; Setayesh, S.; Müllen, K.; Brédas, J. L. *Proc. Natl. Acad. Sci. U.S.A.* **2002**, *99*, 10982. (b) Hennebicq, E.; Pourtois, G.; Scholes, G. D.; Herz, L. M.; Russell, D. M.; Silva, C.; Setayesh, S.; Müllen, K.; Brédas, J. L.; Beljonne, D. *J. Am. Chem. Soc.*, submitted for publication.
(115) Hayes, G. R.; Samuel, I. D. W.; Philipps, R. T. *Phys. Rev. B* **1995**, *52*, 11569.
(116) Harrison, N. T.; Hayes, G. R.; Philipps, R. T.; Friend, R. H. *Phys. Rev. Lett.* **1996**, *77*, 1881.
(117) Brédas, J. L.; Cornil, J.; Heeger, A. J. *Adv. Mater.* **1996**, *8*, 447.
(118) Marcus, R. A. *J. Chem. Phys.* **1965**, *43*, 679.
(119) Guo, D.; Mazumdar, S.; Dixit, S. N.; Kajzar, F.; Jarka, F.; Kawabe, Y.; Peyghambarian, N. *Phys. Rev. B* **1993**, *48*, 1433.
(120) Chen, L.; McBranch, D.; Wang, H.-L.; Hegelson, R.; Wudl, F.; Whitten, D. G. *Proc. Natl. Acad. Sci. U.S.A.* **1999**, *96*, 12287.
(121) (a) Nguyen, T.-Q.; Wu, J.; Doan, V.; Schwartz, B. J.; Tolbert, S. H. *Science* **2000**, *288*, 652. (b) Nguyen, T.-Q.; Wu, J.; Tolbert, S. H.; Schwartz, B. J. *Adv. Mater.* **2001**, *13*, 609.
(122) Yu, J.; Hu, D.; Barbara, P. F. *Science* **2000**, *289*, 1327.
(123) List, E. W. J.; Creely, C.; Leising, G.; Schulte, N.; Schlüter, A. D.; Scherf, U.; Müllen, K.; Graupner, W. *Chem. Phys. Lett.* **2000**, *325*, 132.
(124) Meskers, S. C. J.; Hübner, J.; Oestreich, M.; Bässler, H. *J. Phys. Chem. B* **2001**, *105*, 9139.
(125) Klessinger, M.; Michl, J. *Light Absorption and Photochemistry of Organic Molecules*; VCH: Weinheim, 1993.
(126) Ecoffet, C.; Markovitsi, D.; Millié, P.; Lemaistre, J. P. *Chem. Phys.* **1993**, *177*, 629.
(127) Marguet, S.; Markovitsi, D.; Millié, P.; Sigal, H.; Kumar, S. *J. Phys. Chem. B* **1998**, *102*, 4697.
(128) Krueger, B. P.; Scholes, G. D.; Fleming, G. R. *J. Phys. Chem. B* **1998**, *102*, 5378.
(129) Beljonne, D.; Cornil, J.; Silbey, R.; Millié, P.; Brédas, J. L. *J. Chem. Phys.* **2000**, *112*, 4749.
(130) Beenken, W. J. D.; Pullerits, T. *J. Chem. Phys.* **2004**, *120*, 2490.
(131) Scholes, G. D.; Jordanides, X. J.; Fleming, G. R. *J. Phys. Chem. B* **2001**, *105*, 1640.
(132) Scholes, G. D. *Chem. Phys.* **2001**, *275*, 373.
(133) Karaburnaliev, S.; Bittner, E.; Baumgarten, M. *J. Chem. Phys.* **2001**, *114*, 5863.
(134) Brunner, K.; Tortschanoff, A.; Warmuth, C.; Bässler, H.; Kauffmann, K. F. *J. Phys. Chem. B* **2000**, *104*, 3781.
(135) Dias, F. B.; Maçanita, A. L.; Seixas de Melo, J.; Burrows, H. D.; Güntner, R.; Scherf, U.; Monkman, A. P. *J. Chem. Phys.* **2003**, *118*, 7119.
(136) Setayesh, S.; Marsitzky, D.; Müllen, K. *Macromolecules* **2000**, *33*, 2016.
(137) List, E. J. W.; Scherf, U.; Müllen, K.; Graupner, W.; Kim, C.-H.; Shinar, J. *Phys. Rev. B* **2002**, *66*, 235203.
(138) Hofkens, J.; Cotlet, M.; Vosch, T.; Tinnefeld, P.; Weston, K. D.; Ego, C.; Grimsdale, A.; Müllen, K.; Beljonne, D.; Brédas, J. L.; Jordens, S.; Schweitzer, G.; Sauer, M.; de Schryver, F. C. *Proc. Nat. Acad. Sc. U.S.A.* **2003**, *100*, 13146.
(139) Tessler, N. *Adv. Mater.* **1999**, *11*, 363.
(140) Halls, J. J. M.; Cornil, J.; dos Santos, D. A.; Silbey, R.; Hwang, D. H.; Holmes, A. B.; Brédas, J. L.; Friend, R. H. *Phys. Rev. B* **1998**, *60*, 5721.
(141) Verhoeven, J. W. *Adv. Chem. Phys.* **1999**, *106*, 603.
(142) Jordan, K. D.; Paddon-Row, M. N. *Chem. Rev.* **1992**, *92*, 395.
(143) Adam, D. M.; Brus, L.; Chidsey, C. E. D.; Creager, S.; Creutz, C.; Kagan, C. R.; Kamat, P. V.; Lieberman, M.; Lindsay, S.; Marcus, R. A.; Metzger, R. M.; Michel-Beyerle, M. E.; Miller, J. R.; Newton, M. D.; Rolison, D. R.; Sankey, O.; Schanze, K. S.; Yardley, J.; Zhu, X. *J. Phys. Chem. B* **2003**, *107*, 6668.
(144) Larsson, S.; Volosov, A. *J. Chem. Phys.* **1986**, *85*, 2548.
(145) Filatov, I.; Larsson, S. *Chem. Phys.* **2002**, *284*, 575.
(146) Clayton, A. H. A.; Ghiggino, K. P.; Wilson, G. J.; Paddon-Row, M. N. *J. Phys. Chem.* **1993**, *97*, 7962.
(147) Pourtois, G.; Beljonne, D.; Cornil, J.; Ratner, M. A.; Brédas, J. L. *J. Am. Chem. Soc.* **2002**, *124*, 4436.
(148) Adams, D. M.; Kerimo, J.; Olson, E. J. C.; Zaban, A.; Gregg, B. A.; Barbara, P. F. *J. Am. Chem. Soc.* **1997**, *119*, 10608.
(149) Aroca, R.; Del Cano, T.; de Saja, J. A. *Chem. Mater.* **2003**, *15*, 38 and references therein.
(150) Edwards, L.; Gouterman, M. *J. Mol. Spectrosc.* **1979**, *33*, 292.
(151) Braga, M.; Larsson, S.; Rosen, A.; Volosov, A. *Astron. Astrophys.* **1991**, *245*, 232.
(152) Rhem, D.; Weller, A. *Isr. J. Chem.* **1970**, *8*, 59.
(153) *Handbook of Chemistry and Physics*, 76th ed.; Lide, D. R., Frederikse, H. P. R., Eds.; CRC Press: Boca Raton, 1995.
(154) (a) Cave, R. J.; Newton, M. D. *Chem. Phys. Lett.* **1996**, *249*, 15. (b) Cave, R. J.; Newton, M. D. *J. Chem. Phys.* **1997**, *106*, 9213.
(155) Creutz, C.; Newton, M. D.; Sutin, N. *J. Photochem. Photobiol. A* **1994**, *82*, 47.
(156) Newton, M. D. *Int. J. Quantum Chem.* **2000**, *77*, 255.
(157) van Hal, P. A.; Janssen, R. A. J.; Lanzani, G.; Cerullo, G.; Zavelani-Rossi, M.; De Silvestri, S. *Phys. Rev. B* **2001**, *64*, 075206.
(158) Jenekhe, S. A.; Osaheni, J. A. *Science* **1994**, *265*, 765.
(159) Morteani, A. C.; Dhoot, A. S.; Kim, J. S.; Silva, C.; Greenham, N. C.; Murphy, C.; Moons, E.; Cina, S.; Burroughes, J. H.; Friend, R. H. *Adv. Mater.* **2003**, *15*, 1708.
(160) Arkhipov, V. I.; Heremans, P.; Bässler, H. *Appl. Phys. Lett.* **2003**, *82*, 4605.
(161) Offermans, T.; Meskers, S. C. J.; Janssen, R. A. J. *J. Chem. Phys.* **2003**, *119*, 10924.
(162) Arkhipov, V. I.; Emelianova, V. E.; Bässler, H. *Phys. Rev. Lett.* **1999**, *82*, 1321.
(163) Basko, D. M.; Conwell, E. M. *Phys. Rev. B* **2002**, *66*, 155210.
(164) Neuteboom, E.; Meskers, S. C. J.; van Hal, P. A.; van Duren, J. K. J.; Meijer, E. W.; Janssen, R. A. J.; Dupin, H.; Pourtois, G.; Cornil, J.; Lazzaroni, R.; Brédas, J. L.; Beljonne, D. *J. Am. Chem. Soc.* **2003**, *125*, 8625.

CR040084K